International Journal of Computational Methods
Vol. 6, No. 4 (2009) 633–666

World Scientific
www.worldscientific.com

ADDITIONAL PROPERTIES OF THE NODE-BASED SMOOTHED FINITE ELEMENT METHOD (NS-FEM) FOR SOLID MECHANICS PROBLEMS

T. NGUYEN-THOI[*,‡,§], G. R. LIU[*,†] and H. NGUYEN-XUAN[‡]

[*]*Center for Advanced Computations in Engineering Science (ACES)*
Department of Mechanical Engineering
National University of Singapore, 9 Engineering Drive 1
Singapore 117576, Singapore

[†]*Singapore-MIT Alliance (SMA), E4-04-10*
4 Engineering Drive 3, Singapore, 117576, Singapore

[‡]*Faculty of Mathematics and Computer Science*
University of Sciences
Vietnam National University — HCMC, 227 Nguyen Van Cu
District 5, Hochiminh city, Vietnam
[§]*ngttrung@hcmuns.edu.vn*
[§]*thoitrung76@gmail.com*

Received 26 December 2008
Accepted 15 April 2009

A node-based smoothed finite element method (NS-FEM) for solving solid mechanics problems using a mesh of general polygonal elements was recently proposed. In the NS-FEM, the system stiffness matrix is computed using the smoothed strains over the smoothing domains associated with nodes of element mesh, and a number of important properties have been found, such as the upper bound property and free from the volumetric locking. The examination was performed only for two-dimensional (2D) problems. In this paper, we (1) extend the NS-FEM to three-dimensional (3D) problems using tetrahedral elements (NS-FEM-T4), (2) reconfirm the upper bound and free from the volumetric locking properties for 3D problems, and (3) explore further other properties of NS-FEM for both 2D and 3D problems. In addition, our examinations will be thorough and performed fully using the error norms in both energy and displacement. The results in this work revealed that NS-FEM possesses two additional interesting properties that quite similar to the equilibrium FEM model such as: (1) super accuracy and superconvergence of stress solutions; (2) similar accuracy of displacement solutions compared to the standard FEM model.

Keywords: Numerical methods; meshfree methods; finite element method (FEM); node-based smoothed finite element method (NS-FEM); equilibrium model; compatible model; upper bound; polygonal.

[§]Corresponding author.

1. Introduction

In the development of new numerical methods, Liu *et al.* have applied and extended the strain smoothing technique used in the nodal integrated meshfree methods [Chen *et al.* (2001); Yoo *et al.* (2004)] to formulate the linear conforming point interpolation method (LC-PIM or NS-PIM) [Liu *et al.* (2005)] and the linearly conforming radial point interpolation method (LC-RPIM or NS-RPIM) [Liu *et al.* (2006)]. Applying the same idea to the finite element method (FEM) settings, a cell-based smoothed finite element method (SFEM or CS-FEM) [Liu *et al.* (2007a, b, 2009b); Nguyen-Xuan *et al.* (2008a)], an edge-based smoothed finite element method (ES-FEM) [Liu *et al.* (2009a)], a face-based smoothed finite element method (FS-FEM) [Nguyen-Thoi *et al.* (2009a)], and a node-based smoothed finite element method (NS-FEM) [Liu *et al.* (2009c)] have also been formulated.

In the CS-FEM, the domain discretization is still based on quadrilateral elements as in the FEM; however, the stiffness matrices are calculated based over smoothing domains (SD) located inside the quadrilateral elements as shown in Fig. 1. When the number of SD of the elements equals 1, the CS-FEM solution has the same properties with those of FEM using reduced integration. When SD approaches infinity, the CS-FEM solution approaches the solution of the standard displacement compatible FEM model [Liu *et al.* (2007b)]. In practical computation, using four SD for each quadrilateral element in the CS-FEM is easy to implement, work well in general and hence advised for all problems. The numerical solution of CS-FEM (SD = 4)

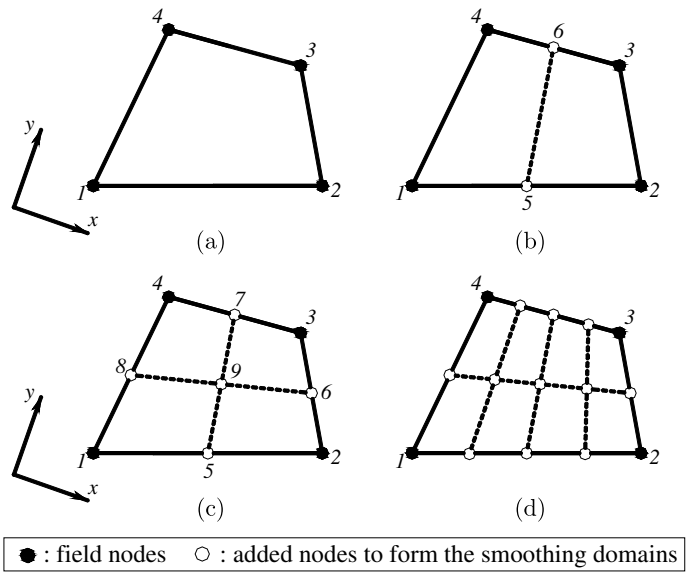

Fig. 1. Division of quadrilateral element into the smoothing domains (SDs) in CS-FEM by connecting the mid-segment-points of opposite segments of smoothing domains; (a) 1 SD; (b) 2 SDs; (c) 4 SDs; and (d) 8 SDs.

is always stable, accurate, much better than that of FEM, and often very close to the exact solutions. The CS-FEM has been extended for general n-sided polygonal elements (nSFEM or nCS-FEM) [Dai *et al.* (2007)], dynamic analyses [Dai and Liu (2007)], incompressible materials using selective integration [Nguyen-Thoi *et al.* (2007); Nguyen-Xuan *et al.* (2008b)], plate and shell analyses [Cui *et al.* (2008); Nguyen-Thanh *et al.* (2008); Nguyen-Van *et al.* (2008); Nguyen-Xuan and Nguyen-Thoi (2009); Nguyen-Xuan and Rabczuk *et al.* (2008c)], and further extended for the extended finite element method (XFEM) to solve fracture mechanics problems in two-dimensional-continuum and plates [Bordas *et al.* (2009)].

In the ES-FEM [Liu and Nguyen-Thoi *et al.* (2009a)], the problem domain is also discretized using triangular elements as in the FEM; however, the stiffness matrices are calculated based on SD associated with the edges of the triangles. For triangular elements, the SD $\Omega^{(k)}$ associated with the edge k is created by connecting two endpoints of the edge to the centroids of the adjacent elements as shown in Fig. 2. The numerical results of ES-FEM using examples of static, free and forced vibration analyses of solids [Liu *et al.* (2009a)] demonstrated the following excellent properties: (1) ES-FEM is often found super-convergent and much more accurate than FEM using triangular elements (FEM-T3) and even more accurate than FEM using quadrilateral elements (FEM-Q4) with the same sets of nodes; (2) there are no spurious nonzeros energy modes and hence ES-FEM is both spatial and temporal stable and works well for vibration analysis; (3) no additional degree of freedom is used; (4) a novel domain-based selective scheme is proposed leading to a combined ES/NS-FEM model that is immune from volumetric locking and hence works very well for nearly incompressible materials. The ES-FEM has been developed for general n-sided polygonal elements (nES-FEM) [Nguyen-Thoi *et al.* (2009b)],

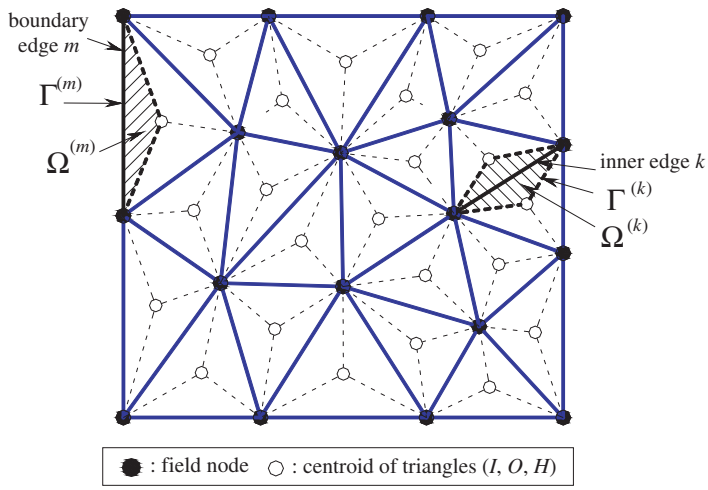

Fig. 2. Triangular elements and the smoothing domains $\Omega^{(k)}$ (shaded areas) associated with edges in the ES-FEM-T3.

2D piezoelectric [Nguyen-Xuan *et al.* (2009a)], 2D visco-elastoplastic [Nguyen-Thoi *et al.* (2009d)], plate [Nguyen-Xuan *et al.* (2009b)], primal-dual shakedown analyses [Tran *et al.* (2009)] and further extended to three-dimensional (3D) problems to give the so-called face-based smoothed finite element method (FS-FEM) [Nguyen-Thoi *et al.* (2009a); Nguyen-Thoi *et al.* (2009e)].

In the NS-FEM, the domain discretization is also based on elements as in the FEM; however, the stiffness matrices are calculated based on SD associated with nodes. The NS-FEM works well for triangular elements, and can be applied easily to general n-sided polygonal elements [Liu *et al.* (2009c)] for 2D problems and tetrahedral elements for 3D problems. For n-sided polygonal elements [Liu *et al.* (2009c)], SD $\Omega^{(k)}$ associated with the node k is created by connecting sequentially the mid-edge-point to the central points of the surrounding n-sided polygonal elements of the node k as shown in Fig. 3. When only linear triangular or tetrahedral elements are used, the NS-FEM produces the same results as the method proposed by [Dohrmann *et al.* (2000)] or to the NS-PIM (or LC-PIM) [Liu *et al.* (2005)] using linear interpolation. The NS-FEM [Liu *et al.* (2009c)] has been found immune naturally from volumetric locking and possesses the upper bound property in strain energy as presented in Liu and Zhang [2008]. Hence, by combining the NS-FEM and FEM with a scale factor $\alpha \in [0, 1]$, a new method named as the alpha Finite Element Method (αFEM) [Liu *et al.* (2008)] is proposed to obtain nearly exact solutions in strain energy using triangular and tetrahedral elements. The NS-FEM has been also developed for adaptive analysis [Nguyen-Thoi *et al.* (2009c)].

However, in the original paper of NS-FEM [Liu *et al.* (2009c)], the properties of the method have not yet been fully exploited. We just considered the upper bound

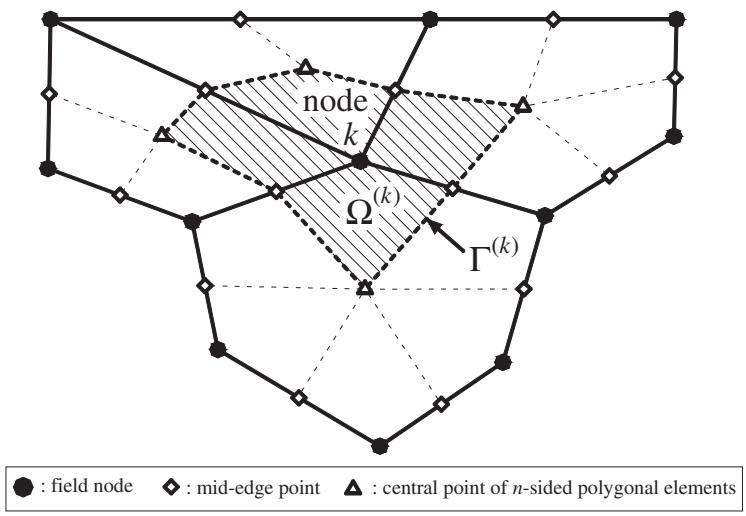

Fig. 3. n-sided polygonal elements and the smoothing domains $\Omega^{(k)}$ (shaded areas) associated with node k.

property in the strain energy and natural immunization from the volumetric locking of the NS-FEM without studying the error and convergence rate of method. In addition, the numerical examples were only applied for 2D problems. In this paper, we therefore further research the additional properties of NS-FEM using triangular elements (NS-FEM-T3) for 2D problems and tetrahedral elements (NS-FEM-T4) for 3D problems by considering fully the error norms in both energy and displacement. The results in this work revealed that NS-FEM possesses two additional interesting properties that quite similar to the equilibrium FEM model [Fraeijs De Veubeke (2001)] such as: (1) super accuracy and super-convergence of stress solutions; (2) similar accuracy of displacement solutions compared to the standard FEM model.

2. Briefing on the NS-FEM

2.1. *Briefing on the finite element method (FEM)* [Bathe (1996); Liu and Quek (2003); Zienkiewicz and Taylor (2000)]

The discrete equations of the FEM are generated from the Galerkin weakform and the integration is performed on the basis of element as follows

$$\int_\Omega (\nabla_s \delta \mathbf{u})^T \mathbf{D} (\nabla_s \mathbf{u}) d\Omega - \int_\Omega \delta \mathbf{u}^T \mathbf{b} d\Omega - \int_{\Gamma_t} \delta \mathbf{u}^T \bar{\mathbf{t}} d\Gamma = 0, \tag{1}$$

where $\mathbf{b}$ is the vector of external body forces, $\mathbf{D}$ is a symmetric positive definite (SPD) matrix of material constants, $\bar{\mathbf{t}}$ is the prescribed traction vector on the natural boundary Γ_t, $\mathbf{u}$ is trial functions, $\delta\mathbf{u}$ is test functions, and $\nabla_s \mathbf{u}$ is the symmetric gradient of the displacement field.

The problem domain Ω is now discretized into N_e of nonoverlapping and nongap elements such that $\Omega = \bigcup_{i=1}^{N_e} \Omega_i^e$ and $\Omega_i^e \cap \Omega_j^e = \varnothing$, $i \neq j$. The FEM then uses the following trial and test functions

$$\mathbf{u}^h(\mathbf{x}) = \sum_{I=1}^{N_n} \mathbf{N}_I(\mathbf{x}) \mathbf{d}_I; \quad \delta\mathbf{u}^h(\mathbf{x}) = \sum_{I=1}^{N_n} \mathbf{N}_I(\mathbf{x}) \delta\mathbf{d}_I, \tag{2}$$

where N_n is the total number of the nodes of the problem domain; $\mathbf{d}_I$ is the nodal displacement vector of Ith node, and $\mathbf{N}_I(\mathbf{x})$ is the shape function matrix at Ith node.

By substituting the approximations, $\mathbf{u}^h$ and $\delta\mathbf{u}^h$, into the weakform and invoking the arbitrariness of virtual nodal displacements, Eq. (1) yields the standard discretized algebraic system of equations:

$$\mathbf{K}^{\mathrm{FEM}} \mathbf{d} = \mathbf{f}, \tag{3}$$

where $\mathbf{K}^{\mathrm{FEM}}$ is the global stiffness matrix, $\mathbf{f}$ is the force vector, that are assembled with entries of

$$\mathbf{K}_{IJ}^{\mathrm{FEM}} = \int_\Omega \mathbf{B}_I^T \mathbf{D} \mathbf{B}_J d\Omega = \sum_{i=1}^{N_e} \int_{\Omega_i^e} \mathbf{B}_I^T \mathbf{D} \mathbf{B}_J d\Omega, \tag{4}$$

$$\mathbf{f}_I = \int_\Omega \mathbf{N}_I^T(\mathbf{x})\mathbf{b}d\Omega + \int_{\Gamma_t} \mathbf{N}_I^T(\mathbf{x})\bar{\mathbf{t}}d\Gamma, \tag{5}$$

with the *compatible strain–displacement matrix* defined as

$$\mathbf{B}_I(\mathbf{x}) = \nabla_s \mathbf{N}_I(\mathbf{x}). \tag{6}$$

Using the triangular/tetrahedral elements with the linear shape functions, the compatible strain–displacement matrix $\mathbf{B}_I(\mathbf{x})$ contains only constant entries. Equation (4) then becomes

$$\mathbf{K}_{IJ}^{\text{FEM}} = \sum_{i=1}^{N_e} \mathbf{B}_I^T \mathbf{D}\mathbf{B}_J S_i^e, \tag{7}$$

where $S_i^e \equiv A_i^e = \int_{\Omega_i^e} d\Omega$ is the area of the triangular element, or $S_i^e \equiv V_i^e = \int_{\Omega_i^e} d\Omega$ is the volume of the tetrahedral element.

2.2. *The NS-FEM based on triangular elements (NS-FEM-T3) for 2D problems*

The NS-FEM for 2D problems works for polygonal elements of arbitrary sides [Liu *et al.* (2009c)]. Here we brief only the formulation for triangular element (NS-FEM-T3).

Similar to the FEM, the NS-FEM also uses a mesh of elements. When three-node triangular elements are used, the shape functions used in the NS-FEM-T3 are also identical to those in the FEM-T3, and hence the displacement field in the NS-FEM-T3 is also ensured to be continuous on the whole problem domain. However, being different from the FEM-T3 which performs the integration required in Eq. (1) on the elements, NS-FEM-T3 performs the integration based on the nodes, and strain smoothing technique [Chen *et al.* (2001)] is used. In such a nodal integration process, the problem domain Ω is divided into N_n SD $\Omega^{(k)}$ associated with nodes k such that $\Omega = \sum_{k=1}^{N_n} \Omega^{(k)}$ and $\Omega^{(i)} \cap \Omega^{(j)} = \varnothing$, $i \neq j$. For triangular elements, the SD $\Omega^{(k)}$ associated with the node k is created by connecting sequentially the mid-edge-points to the centroids of the surrounding triangular elements of the node k as shown in Fig. 4. As a result, each triangular element will be subdivided into three quadrilateral sub-domains and each quadrilateral sub-domain is attached with the nearest field node. The SD $\Omega^{(k)}$ associated with the node k is then created by combination of each nearest quadrilateral sub-domain of all elements surrounding the node k.

Using the node-based smoothing operation to smooth the compatible strain $\boldsymbol{\varepsilon}^h = \nabla_s \mathbf{u}^h$ on the SD $\Omega^{(k)}$ associated with node k, the strain in Eq. (1) now becomes the *smoothed* strain $\bar{\boldsymbol{\varepsilon}}_k$ on $\Omega^{(k)}$:

$$\bar{\boldsymbol{\varepsilon}}_k = \int_{\Omega^{(k)}} \boldsymbol{\varepsilon}^h(\mathbf{x})\Phi_k(\mathbf{x})d\Omega = \int_{\Omega^{(k)}} \nabla_s \mathbf{u}^h(\mathbf{x})\Phi_k(\mathbf{x})d\Omega, \tag{8}$$

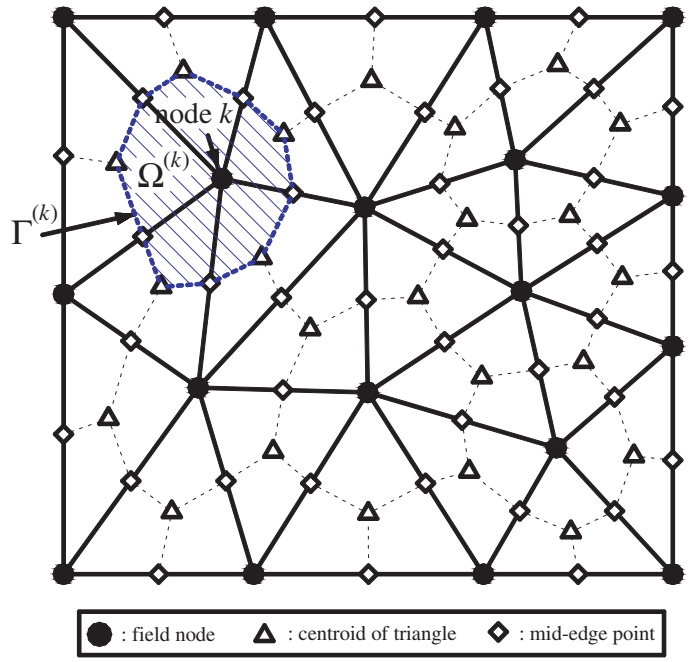

Fig. 4. Triangular elements and smoothing domains $\Omega^{(k)}$ (shaded area) associated with the nodes in the NS-FEM-T3.

where $\Phi_k(\mathbf{x})$ is a given smoothing function that satisfies at least unity property

$$\int_{\Omega^{(k)}} \Phi_k(\mathbf{x}) d\Omega = 1. \tag{9}$$

Using the following constant smoothing function

$$\Phi_k(\mathbf{x}) = \begin{cases} 1/A^{(k)} & \mathbf{x} \in \Omega^{(k)}, \\ 0 & \mathbf{x} \notin \Omega^{(k)}, \end{cases} \tag{10}$$

where $A^{(k)} = \int_{\Omega^{(k)}} d\Omega$ is the area of the SD $\Omega^{(k)}$.

Substituting Eqs. (2) and (10) into Eq. (8), the smoothed strain on the SD $\Omega^{(k)}$ associated with node k can be written in the following matrix form of nodal displacements

$$\bar{\boldsymbol{\varepsilon}}_k = \sum_{I \in N_n^{(k)}} \bar{\mathbf{B}}_I(\mathbf{x}_k)\mathbf{d}_I, \tag{11}$$

where $N_n^{(k)}$ is the number of nodes that are directly connected to node k and $\bar{\mathbf{B}}_I(\mathbf{x}_k)$ is termed as the smoothed strain–displacement matrix on the SD $\Omega^{(k)}$. As presented in the original paper of NS-FEM [Liu *et al.* (2009c)], there are two ways to compute the matrix $\bar{\mathbf{B}}_I(\mathbf{x}_k)$. In the first general way, the integration along the boundary of SD and the values of shape functions are directly used, which works for general n-sided

polygonal elements including linear triangular elements. In the second particular way, the smoothed strain–displacement matrix is the area-weighted average of the compatible strain–displacement matrices of elements associated with the computed node, which works only for linear triangular elements. In this paper, we use the second simple way only for three-node triangular elements as follows

$$\bar{\mathbf{B}}_I(\mathbf{x}_k) = \frac{1}{A^{(k)}} \sum_{j=1}^{N_e^{(k)}} \frac{1}{3} A_e^{(j)} \mathbf{B}_j^e, \tag{12}$$

where $N_e^{(k)}$ is the number of elements around node k; $A_e^{(j)}$ is the area of the jth triangular element around node k; $A^{(k)}$ is the area of the SD $\Omega^{(k)}$ associated with node k and computed using

$$A^{(k)} = \int_{\Omega^{(k)}} d\Omega = \frac{1}{3} \sum_{j=1}^{N_e^{(k)}} A_e^{(j)}. \tag{13}$$

In Eq. (12), matrix $\mathbf{B}_j^e = \sum_{I \in S_j^e} \mathbf{B}_I$ is the compatible strain–displacement matrix for the jth triangular element around the node k. It is assembled from the compatible strain–displacement matrices $\mathbf{B}_I(\mathbf{x})$ of nodes by Eq. (6) in the set S_j^e which contains three nodes of the jth triangular element.

The stiffness matrix $\bar{\mathbf{K}}$ of the system is then assembled by a similar process as in the FEM

$$\bar{\mathbf{K}}_{IJ} = \sum_{k=1}^{N_n} \bar{\mathbf{K}}_{IJ}^{(k)}, \tag{14}$$

where $\bar{\mathbf{K}}_{IJ}^{(k)}$ is the stiffness matrix associated with node k and is calculated by

$$\bar{\mathbf{K}}_{IJ}^{(k)} = \int_{\Omega^{(k)}} \bar{\mathbf{B}}_I^T \mathbf{D} \bar{\mathbf{B}}_J d\Omega = \bar{\mathbf{B}}_I^T \mathbf{D} \bar{\mathbf{B}}_J A^{(k)}. \tag{15}$$

2.3. *The NS-FEM based on tetrahedral elements (NS-FEM-T4) for 3D problems*

The above formulation is quite straightforward to extend for 3D problems using four-node tetrahedral elements (T4) [Liu *et al.* (2009c)]. The smoothed strain–displacement matrix $\bar{\mathbf{B}}_I(\mathbf{x}_k)$ for the NS-FEM-T4 is assembled using

$$\bar{\mathbf{B}}_I(\mathbf{x}_k) = \frac{1}{V^{(k)}} \sum_{j=1}^{N_e^{(k)}} \frac{1}{4} V_e^{(j)} \mathbf{B}_j^e, \tag{16}$$

where $V_e^{(j)}$ is the volume of the jth tetrahedral element around the node k; $V^{(k)}$ is the volume of the SD $\Omega^{(k)}$ associated with node k, and is computed using

$$V^{(k)} = \int_{\Omega^{(k)}} d\Omega = \frac{1}{4} \sum_{j=1}^{N_e^{(k)}} V_e^{(j)}. \tag{17}$$

In Eq. (16), matrix $\mathbf{B}_j^e = \sum_{I \in S_j^e} \mathbf{B}_I$ is the compatible strain–displacement matrix for the jth tetrahedral element around the node k. It is assembled from the compatible strain–displacement matrices $\mathbf{B}_I(\mathbf{x})$ of nodes by Eq. (6) in the set S_j^e which contains four nodes of the jth tetrahedral element.

With such the formulation, only the area/volume and the usual compatible strain–displacement matrices $\mathbf{B}_j^e$ of triangular/tetrahedral elements are needed to calculate the system stiffness matrix for the NS-FEM-T3/NS-FEM-T4. The formulation is simple, but works only for triangular/tetrahedral types of elements that use linear interpolation.

2.4. *A brief of properties of the NS-FEM*

The following properties of the NS-FEM were presented by Liu *et al.* [2009c]. In this paper, we only remind the main points.

Property 1. The NS-FEM can be derived straightforwardly from the modified Hellinger-Reissner variational principle, with the smoothed strain vector $\bar{\boldsymbol{\varepsilon}}_k$ and displacements $\mathbf{u}^h(\mathbf{x})$ as independent field variables, to give the stiffness matrix associated with nodes $\bar{\mathbf{K}}_{IJ}^{(k)}$ in the form of Eqs. (14) and (15). The method is therefore variationally consistent.

Property 2. The strain energy $E(\mathbf{d})$ obtained from the NS-FEM solution has the following relationship with the exact strain energy:

$$E(\mathbf{d}) \geq E_{\text{exact}}(\mathbf{d}_0), \tag{18}$$

where $\mathbf{d}$ is the numerical solution of the NS-FEM, and $\mathbf{d}_0$ is the exact displacement sampled using the exact displacement field $\mathbf{u}_0$.

Property 3. The NS-FEM possesses only "legal" zero energy modes that represents the rigid motions, and there exists no spurious zero energy mode.

Property 4. The NS-FEM is immune naturally from the volumetric locking.

3. Error Norms in Displacement and Energy

In the original paper of NS-FEM [Liu *et al.* (2009c)], the properties of the method have not yet been fully exploited. In [Liu *et al.* [2009c], we just considered the upper bound property in the strain energy and natural immunization from the volumetric locking of the NS-FEM without studying the error and convergence rate of method. In addition, the numerical examples were only applied for 2D problems. In next section, we (1) extend the NS-FEM to 3D problems using tetrahedral elements (NS-FEM-T4), (2) reconfirm the upper bound and free from the volumetric locking properties for 3D problems, and (3) explore further other properties of NS-FEM for both 2D and 3D problems by considering fully the error norms in both energy and displacement.

To demonstrate clearly the properties of the NS-FEM, we will compare the results of NS-FEM with those of some existing methods. For 2D problems, the results of the NS-FEM using three-node triangular elements (NS-FEM-T3) will be compared with those of the standard FEM using quadrilateral elements (FEM-Q4), triangular elements (FEM-T3), and the edge-based smoothed FEM using three-node triangular elements (ES-FEM-T3) [Liu *et al.* (2009a)]. The results of the NS-FEM using tetrahedral elements (NS-FEM-T4) will be compared with those of the standard displacement FEM using four-node tetrahedral elements (FEM-T4), eight-node hexahedral elements (FEM-H8), and the face-based smoothed FEM using four-node tetrahedral elements (FS-FEM-T4) [Nguyen-Thoi *et al.* (2009a)].

3.1. *Displacement norm*

Let $\breve{\mathbf{u}}$ be the numerical solution for displacement obtained using any numerical method. For example, for the FEM, $\breve{\mathbf{u}} = \mathbf{u}^h$, for the S-FEM models (NS-FEM, ES-FEM, and FS-FEM), $\breve{\mathbf{u}} = \bar{\mathbf{u}}$, then the displacement norm used in this paper is defined as

$$e_d = \left(\int_\Omega (\mathbf{u} - \breve{\mathbf{u}})^T (\mathbf{u} - \breve{\mathbf{u}})\, d\Omega \right)^{1/2} = \left(\sum_{i=1}^{N_e} \int_{\Omega_i^e} (\mathbf{u} - \breve{\mathbf{u}})^T (\mathbf{u} - \breve{\mathbf{u}})\, d\Omega \right)^{1/2}, \quad (19)$$

where $\mathbf{u}$ is the exact or analytical solution for the displacement.

3.2. *Energy norm*

Let $\breve{\boldsymbol{\varepsilon}}$ be the numerical solution for strains obtained using any numerical method. For example, for the FEM, $\breve{\boldsymbol{\varepsilon}} = \boldsymbol{\varepsilon}^h$, for the S-FEM models (NS-FEM, ES-FEM, and FS-FEM), $\breve{\boldsymbol{\varepsilon}} = \bar{\boldsymbol{\varepsilon}}$, then the energy norm is defined by

$$e_e = \left[\int_\Omega \frac{1}{2} (\boldsymbol{\varepsilon} - \breve{\boldsymbol{\varepsilon}})^T \mathbf{D} (\boldsymbol{\varepsilon} - \breve{\boldsymbol{\varepsilon}}) \right]^{1/2} = \left[\sum_{i=1}^{N_e} \int_{\Omega_i^e} \frac{1}{2} (\boldsymbol{\varepsilon} - \breve{\boldsymbol{\varepsilon}})^T \mathbf{D} (\boldsymbol{\varepsilon} - \breve{\boldsymbol{\varepsilon}}) \right]^{1/2}, \quad (20)$$

where $\boldsymbol{\varepsilon}$ is the exact or analytical solution for the strain.

In order to evaluate the integrals in Eqs. (19) and (20) accurately, the mapping procedure using Gauss integration rule is performed on each element Ω_i^e. In each element, a proper number of Gauss points depending on the order of the integrand will be used. For example in Eq. (20), when a quadrilateral mesh of FEM-Q4 elements are used, and if the analytical strain $\boldsymbol{\varepsilon}$ is of order of 2 leading to a fourth-order integrand, a set of 3×3 Gauss points are then used for each element.

3.3. *Recovery strain fields for smoothed FEM models (S-FEM)*

In the S-FEM models (NS-FEM, ES-FEM, and FS-FEM), the strain obtained within an element is piecewise constants and discontinuous at the boundaries of smoothing

domains located inside elements. Therefore, it is necessary to create a continuous strain field within each element for easy evaluation of the integrals in Eq. (20). In this paper, we construct a "recovery" strain field denoted as $\bar{\boldsymbol{\varepsilon}}_R$ by combining the strain values $\bar{\boldsymbol{\varepsilon}}$ at the nodes of the element and shape functions of the standard FEM. Such a recovery strain field $\bar{\boldsymbol{\varepsilon}}_R$ is not only continuous inside the element, but also on the whole problem domain, and will be used as the final numerical strain field for the S-FEM models, and in the error estimation by Eq. (20).

For the S-FEM models using triangular, quadrilateral, and tetrahedral elements, $\bar{\boldsymbol{\varepsilon}}_R$ is obtained for each element using

$$\bar{\boldsymbol{\varepsilon}}_R = \sum_{j=1}^{n_n^e} N_j(\mathbf{x})\bar{\boldsymbol{\varepsilon}}(\mathbf{x}_j), \tag{21}$$

where n_n^e is the number of the nodes of each element, $\bar{\boldsymbol{\varepsilon}}(\mathbf{x}_j)$ is the strain at the nodes $\mathbf{x}_j$ of the element obtained using the S-FEM models; and $N_j(\mathbf{x})$ is the matrix of shape functions of the corresponding elements used in the standard FEM. Specifically, for the triangular elements, the three-node linear shape function is used. For tetrahedral elements, the four-node linear shape function is used. For the quadrilateral elements, the bilinear shape function is used.

3.4. *Evaluation of strains at nodes in the S-FEM models*

In the numerical implementation of the S-FEM models, except the NS-FEM which produces directly the strain values at nodes, the strains at the node j will be the (area-weighted) averaged value of the "raw" strains of the SD $\Omega^{(k)}$ around node j, and are computed numerically by

$$\begin{aligned}
\bar{\boldsymbol{\varepsilon}}(\mathbf{x}_j) &= \tfrac{1}{A_j^{ns}} \sum_{k=1}^{n_s^j} \bar{\boldsymbol{\varepsilon}}_k A^{(k)}, \quad \text{for ES-FEM-T3,} \\
\bar{\boldsymbol{\varepsilon}}(\mathbf{x}_j) &= \tfrac{1}{V_j^{ns}} \sum_{k=1}^{n_s^j} \bar{\boldsymbol{\varepsilon}}_k V^{(k)}, \quad \text{for FS-FEM-T4,}
\end{aligned} \tag{22}$$

where n_s^j is the number of SD $\Omega^{(k)}$ around node j; $A_j^{ns} = \sum_{k=1}^{n_s^j} A^{(k)}$ and $V_j^{ns} = \sum_{k=1}^{n_s^j} V^{(k)}$ are, respectively, the total area and volume of all SD $\Omega^{(k)}$ around the node j; $\bar{\boldsymbol{\varepsilon}}_k$ is the smoothing strain of the SD $\Omega^{(k)}$; and $A^{(k)}$ and $V^{(k)}$ are, respectively, the area and volume of the SD $\Omega^{(k)}$. Figure 5 shows, for example, used to compute strain of the nodes in the ES-FEM-T3 using three-node triangular elements.

3.5. *Recovery strain/stress fields for FEM models*

For FEM models, the compatible strains in the elements are already continuous, Eq. (20) hence can be evaluated directly without using a recovery strain field. In

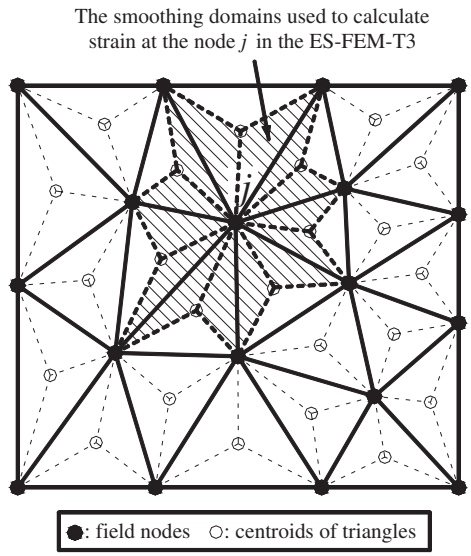

Fig. 5. Smoothing domains used to compute strain of the nodes in the ES-FEM-T3 using three-node triangular elements.

addition, using such compatible strains in Eq. (20), the theoretical convergence rates of the standard FEM can be illustrated clearly in figures and are the good bases to evaluate the accuracy and efficiency of others compared numerical methods. Specifically, for the standard lower-order elements such as FEM-T3, FEM-Q4, FEM-T4, and FEM-H8, the theoretical convergence rates of displacement norm and energy norm are, respectively, 2 and 1.

In this paper, in addition to using the compatible strain for the standard FEM, we also use the recovery strain $\boldsymbol{\varepsilon}_R^h$ for the FEM models (FEM-T3-Re, FEM-Q4-Re, FEM-T4-Re, and FEM-H8-Re) to be able to conduct "fairest" possible comparisons between the S-FEM and FEM models. It is because the recovery strain solutions are much more accurate for FEM models, and have the supper-convergence property [Zienkiewicz and Zhu (1992a, b)]. The recovery strain solution $\boldsymbol{\varepsilon}_R^h$ is obtained using

$$\boldsymbol{\varepsilon}_R^h = \sum_{j=1}^{n_n^e} N_j(\mathbf{x})\boldsymbol{\varepsilon}^h(\mathbf{x}_j). \tag{23}$$

It is clear that Eq. (23) is exactly the same as Eq. (21), except that $\boldsymbol{\varepsilon}^h(\mathbf{x}_j)$ is the strain at the nodes $\mathbf{x}_j$ of the element obtained using the FEM model. For triangular and tetrahedral elements (FEM-T3-Re and FEM-T4-Re), the strain $\boldsymbol{\varepsilon}^h(\mathbf{x}_j)$ at the node $\mathbf{x}_j$ is the area-weighted average of the strains of elements surrounding the node $\mathbf{x}_j$ [Zienkiewicz and Zhu (1992a, b)]. For the quadrilateral and hexahedral elements (FEM-Q4-Re, FEM-H8-Re), the strain $\boldsymbol{\varepsilon}^h(\mathbf{x}_j)$ at the node $\mathbf{x}_j$ is computed by the

following three-step procedure [Felippa (2009)]:

(1) Evaluate the strains at the Gauss points in the element.
(2) Extrapolate the strains at Gauss points to the nodes of the element.
(3) Average the strains computed for the same field node from the adjacent elements.

3.6. *Characteristic length*

To evaluate the convergence rates of the displacement and energy norms, it is necessary to define the "characteristic length" of the sides of the elements. In this paper, because the elements used in a mesh are different in dimensions and of irregular shape, the average length h of sides of elements is considered to be the characteristic length. For the quadrilateral elements, h is evaluated by

$$h = \sqrt{\frac{A_\Omega}{N_e}}, \tag{24}$$

where A_Ω is the area of the whole problem domain. For the triangular elements, h is evaluated by

$$h = \sqrt{\frac{2A_\Omega}{N_e}}. \tag{25}$$

For the tetrahedral elements, h is evaluated by

$$h = \sqrt[3]{\frac{6V_\Omega}{N_e}}, \tag{26}$$

and for the hexahedral elements (just used for FEM-H8), h is evaluated by

$$h = \sqrt[3]{\frac{V_\Omega}{N_e}}, \tag{27}$$

where V_Ω is the volume of the whole problem domain.

4. Numerical Examples

4.1. *A rectangular cantilever loaded at the end*

A rectangular cantilever with a length L and height D is studied as a benchmark problem here. The cantilever is subjected to a parabolic traction at the free end as shown in Fig. 6. The beam is assumed to have a unit thickness so that plane stress condition is valid. The analytical solution is available and can be found in a textbook [Timoshenko and Goodier (1970)].

$$\begin{aligned} u_x &= \frac{Py}{6EI}\left[(6L-3x)x + (2+\nu)\left(y^2 - \frac{D^2}{4}\right)\right] \\ u_y &= -\frac{P}{6EI}\left[3\nu y^2(L-x) + (4+5\nu)\frac{D^2 x}{4} + (3L-x)x^2\right] \end{aligned} \tag{28}$$

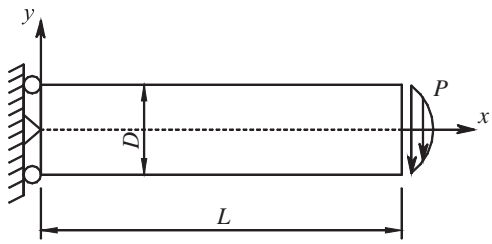

Fig. 6. Cantilever loaded at the end.

where the moment of inertia I for a beam with rectangular cross section and unit thickness is given by $I = \frac{D^3}{12}$.

The stresses corresponding to the displacements Eq. (28) are

$$\sigma_{xx}(x,y) = \frac{P(L-x)y}{I}; \quad \sigma_{yy}(x,y) = 0; \quad \tau_{xy}(x,y) = -\frac{P}{2I}\left(\frac{D^2}{4} - y^2\right) \tag{29}$$

The related parameters are taken as $E = 3.0 \times 10^7\,\mathrm{N/m^2}$, $\nu = 0.3$, $D = 12\,\mathrm{m}$, $L = 48\,\mathrm{m}$ and $P = 1000\,\mathrm{N}$. The domain of the beam is discretized into two types of meshes using two different elements: three-node triangular and four-node quadrilateral elements are shown in Fig. 7. The exact strain energy of the problem is known as 4.4747 Nm.

The numerical results of strain energy are presented in Table 1, and plotted in Fig. 8 against the degrees of freedom, revealing the convergence of the solution of

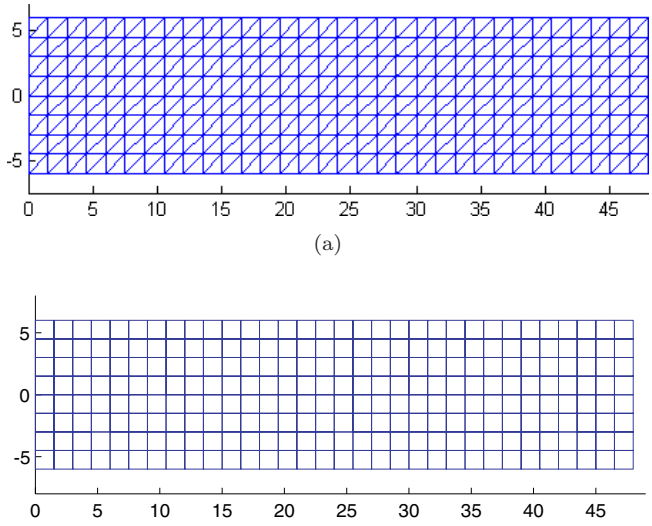

Fig. 7. Domain discretization of the cantilever using: (a) three-node triangular elements; (b) four-node quadrilateral elements.

Table 1. Strain energy (Nm) obtained using different methods for the cantilever problem using the same set of nodes.

	Mesh 16×4	Mesh 24×6	Mesh 32×8	Mesh 40×10	Mesh 48×12	Analytical solution
DOFs	170	350	694	902	1274	
FEM-T3	3.7134	4.0973	4.2533	4.3301	4.3731	4.4747
FEM-Q4	4.3362	4.4118	4.4390	4.4518	4.4587	4.4747
NS-FEM-T3	4.9785	4.7031	4.6051	4.5591	4.5338	4.4747
ES-FEM-T3	4.4097	4.4539	4.4654	4.4697	4.4717	4.4747

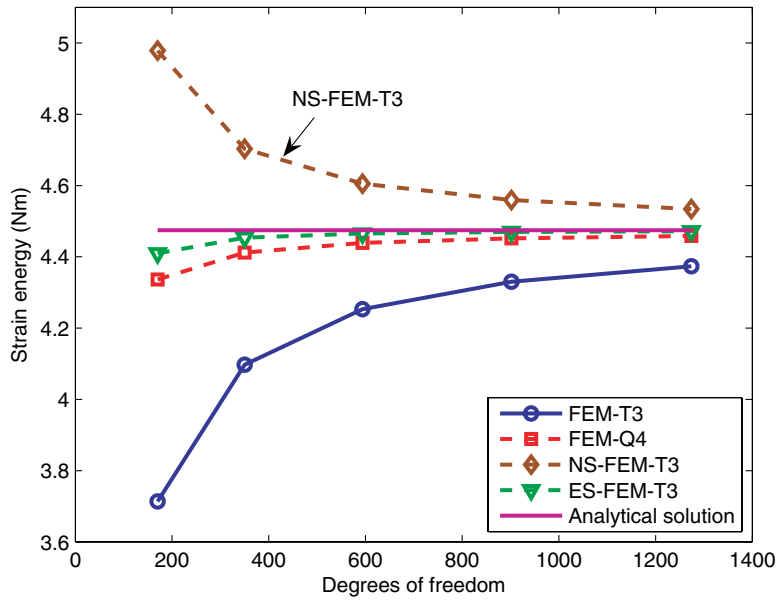

Fig. 8. Convergence of the strain energy solution of the NS-FEM-T3 in comparison with other methods for the cantilever problem using the same set of nodes.

all models used. It can be found that the NS-FEM-T3 gives upper bound solutions in the strain energy, i.e. the strain energies of the NS-FEM-T3 are always bigger than the exact one and converge to it with the increase of degrees of freedom. In contrast, the FEM-Q4 and FEM-T3 produce the lower bound solutions in the strain energy. These results imply that we now have a very simple procedure to determine upper and lower bounds in strain energy of the exact solution, by using the NS-FEM together the FEM using the same meshes.

Table 2 and Fig. 9 compare the solution error in displacement norm obtained using the NS-FEM-T3, together with those of the FEM-T3, FEM-Q4, and ES-FEM-T3. It is seen that the ES-FEM-T3 stands out clearly. The error of displacement norm of the ES-FEM-T3 is the smallest among all the compared models. When

Table 2. Error in displacement norm obtained using different methods for the cantilever problem using the same set of nodes.

	Mesh 16×4	Mesh 24×6	Mesh 32×8	Mesh 40×10	Mesh 48×12
h (m)	4.0	2.0	1.5	1.2	1.0
FEM-T3	1.78 e-02	8.80 e-03	5.16 e-03	3.36 e-03	2.36 e-03
FEM-Q4	2.97 e-03	1.35 e-03	7.63 e-04	4.90 e-04	3.41 e-04
NS-FEM-T3	1.23 e-02	5.60 e-03	3.20 e-03	2.07 e-03	1.45 e-03
ES-FEM-T3	1.32 e-03	3.74 e-04	1.47 e-04	6.94 e-05	3.68 e-05

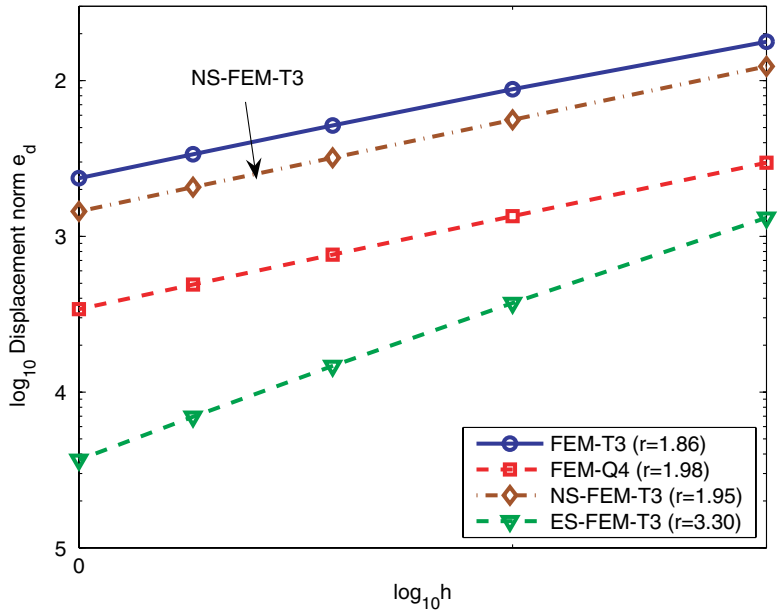

Fig. 9. Error in displacement norm for the NS-FEM solution in comparison with that of other methods for the cantilever problem using the same set of nodes.

the finest mesh ($h = 1$ m) is used, the error of the ES-FEM-T3 is about 1/5 of the FEM-T3 and 3/4 of the FEM-Q4. The error of the NS-FEM-T3 is about 3/5 of the FEM-T3. In terms of convergence rate, the super-convergence is observed for the ES-FEM-T3 with a rate of 3.3 that is even much higher than the theoretical value of 2.0 for linear displacement models based on the weak formulation. The convergence rates of others methods, except the FEM-T3, are approximated to the theoretical value of 2.0 for linear displacement models.

Table 3 and Fig. 10 compare the results of energy norm of the NS-FEM-T3, together with those of the FEM and ES-FEM-T3. It is seen that the NS-FEM-T3 stands out clearly. When the finest mesh ($h = 1$ m) is used, the error of the NS-FEM-T3 solution is about 1/8 of the FEM-T3, 1/3 of the FEM-Q4 and even

Table 3. Error in energy norm obtained using different methods for the cantilever problem using the same set of nodes.

	Mesh 16×4	Mesh 24×6	Mesh 32×8	Mesh 40×10	Mesh 48×12
h (m)	4.0	2.0	1.5	1.2	1.0
FEM-T3	8.77 e-01	6.16 e-01	4.71 e-01	3.80 e-01	3.18 e-01
FEM-Q4	3.71 e-01	2.49 e-01	1.88 e-01	1.50 e-01	1.25 e-01
NS-FEM-T3	1.44 e-01	9.45 e-02	6.71 e-02	5.06 e-02	3.99 e-02
ES-FEM-T3	2.96 e-01	1.58 e-01	1.02 e-01	7.28 e-02	5.53 e-02
FEM-T3-Re	5.76 e-01	3.04 e-01	1.87 e-01	1.28 e-01	9.34 e-02
FEM-Q4-Re	2.06 e-01	1.14 e-01	7.49 e-02	5.38 e-02	4.10 e-02

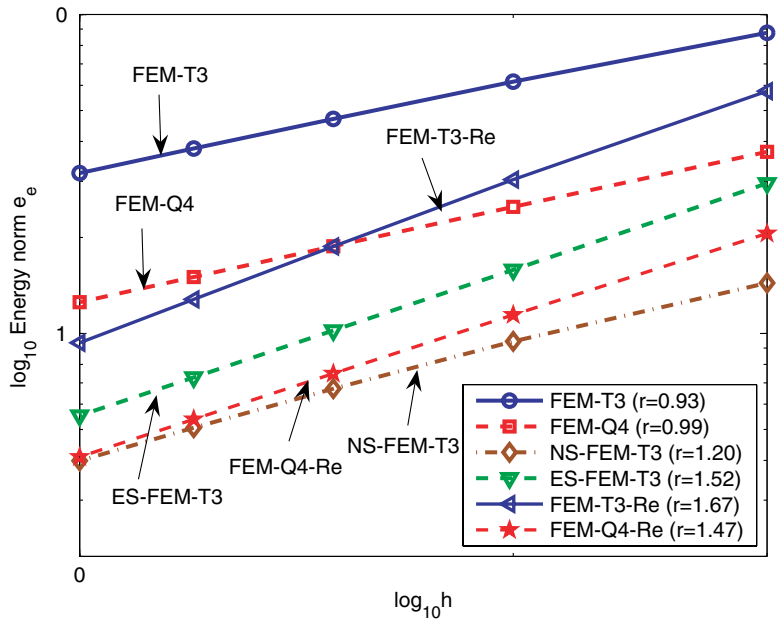

Fig. 10. Error in energy norm for the NS-FEM solution in comparison with those of other methods for the cantilever problem using the same set of nodes.

better than the FEM-Q4-Re. In terms of convergence rate, all the S-FEM models performed much better than the standard FEM models, and all significantly above 1.0 that is the theoretical value of the weak formulation. This shows that the S-FEM models are super-convergent. NS-FEM-T3 has a rate of 1.2: a quite strong super-convergence.

From this example, we also note that the NS-FEM-T3 possesses three interesting properties similar to those of an equilibrium FEM model [Almeida Pereira (2008); Debongnie *et al.* (1995); Fraeijs De Veubeke (2001)]: (1) the strain energy is an upper bound of the exact solution; (2) the stress solutions are ultra-accurate and

super-convergent; and (3) the displacement solutions are not so significantly more accurate but are still better than that of FEM-T3.

4.2. *Infinite plate with a circular hole*

Figure 11 represents a plate with a central circular hole of radius $a = 1\,\text{m}$, subjected to a unidirectional tensile load of $1.0\,\text{N/m}$ at infinity in the x-direction. Due to its symmetry, only the upper right quadrant of the plate is modeled. Figure 12 gives the discretization of the domain using three-node triangular and four-node quadrilateral elements. Plane strain condition is considered and $E = 1.0\times10^3\,\text{N/m}^2$, $\nu = 0.3$. Symmetric conditions are imposed on the left and bottom edges, and the inner boundary of the hole is traction free. The exact stresses for this problem are

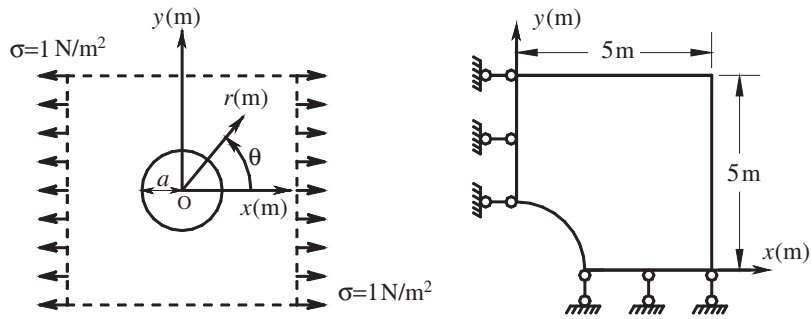

Fig. 11. Infinite plate with a circular hole subjected to unidirectional tension and its quarter model with symmetric conditions imposed on the left and bottom edges.

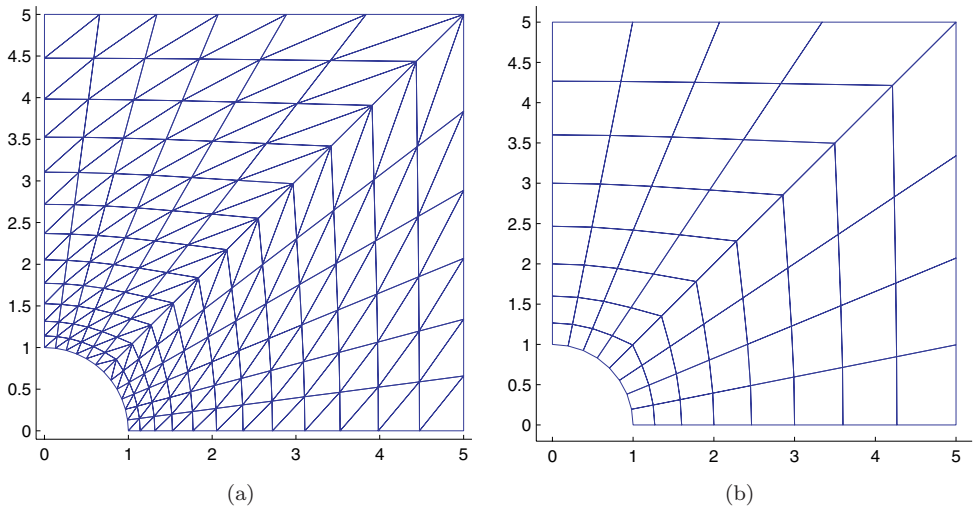

Fig. 12. Domain discretization of the infinite plate with a circular hole using (a) three-node triangular elements; (b) four-node quadrilateral elements.

[Timoshenko and Goodier (1970)]

$$\begin{aligned}
\sigma_{11} &= 1 - \frac{a^2}{r^2}\left[\frac{3}{2}\cos 2\theta + \cos 4\theta\right] + \frac{3a^4}{2r^4}\cos 4\theta,\\
\sigma_{22} &= -\frac{a^2}{r^2}\left[\frac{1}{2}\cos 2\theta - \cos 4\theta\right] - \frac{3a^4}{2r^4}\cos 4\theta,\\
\tau_{12} &= -\frac{a^2}{r^2}\left[\frac{1}{2}\sin 2\theta + \sin 4\theta\right] + \frac{3a^4}{2r^4}\sin 4\theta,
\end{aligned} \tag{30}$$

where (r, θ) are the polar coordinates and θ is measured counterclockwise from the positive x-axis. Traction boundary conditions are imposed on the right ($x = 5\,\mathrm{m}$) and top ($y = 5\,\mathrm{m}$) edges based on the exact solution Eq. (30). The displacement components corresponding to the stresses are

$$\begin{aligned}
u_1 &= \frac{a}{8\mu}\left[\frac{r}{a}(\kappa+1)\cos\theta + 2\frac{a}{r}((1+\kappa)\cos\theta + \cos 3\theta) - 2\frac{a^3}{r^3}\cos 3\theta\right],\\
u_2 &= \frac{a}{8\mu}\left[\frac{r}{a}(\kappa-3)\sin\theta + 2\frac{a}{r}((1-\kappa)\sin\theta + \sin 3\theta) - 2\frac{a^3}{r^3}\sin 3\theta\right],
\end{aligned} \tag{31}$$

where $\mu = E/(2(1+\nu))$, κ is defined in terms of Poisson's ratio by $\kappa = 3 - 4\nu$ for plane strain cases. The exact strain energy of the problem is known as $1.1817 \times 10^{-2}\,\mathrm{Nm}$.

The numerical results of strain energy have been presented in Table 4 and plotted in Fig. 13 against the degrees of freedom, revealing the convergence of the solution of all models used. It again shows the upper bound property in the strain energy of the NS-FEM-T3, together with the lower bound property of the FEM-Q4 and FEM-T3.

Table 5 and Fig. 14 compare the results of displacement norm of the NS-FEM-T3 with those of the FEM and ES-FEM-T3. It is again seen that the ES-FEM-T3 stands out clearly. The error of displacement norm of the ES-FEM-T3 is the smallest among all the compared models. When the finest mesh ($h = 0.1969\mathrm{m}$) is used, the error of the ES-FEM-T3 is about 1/5 of the FEM-T3, 3/4 of the FEM-Q4. The NS-FEM-T3 performed better than the FEM-T3, but only by a small margin. In

Table 4. Strain energy ($\times 10^{-2}\,\mathrm{Nm}$) using different methods for the infinite plate with a circular hole using the same set of nodes.

	Mesh 12×12	Mesh 16×16	Mesh 20×20	Mesh 24×24	Analytical solution
DOFs	338	578	882	1250	
FEM-T3	1.1762	1.1786	1.1797	1.1803	1.1817
FEM-Q4	1.1794	1.1805	1.1810	1.1812	1.1817
NS-FEM-T3	1.1848	1.1834	1.1827	1.1824	1.1817
ES-FEM-T3	1.1804	1.1811	1.1814	1.1815	1.1817

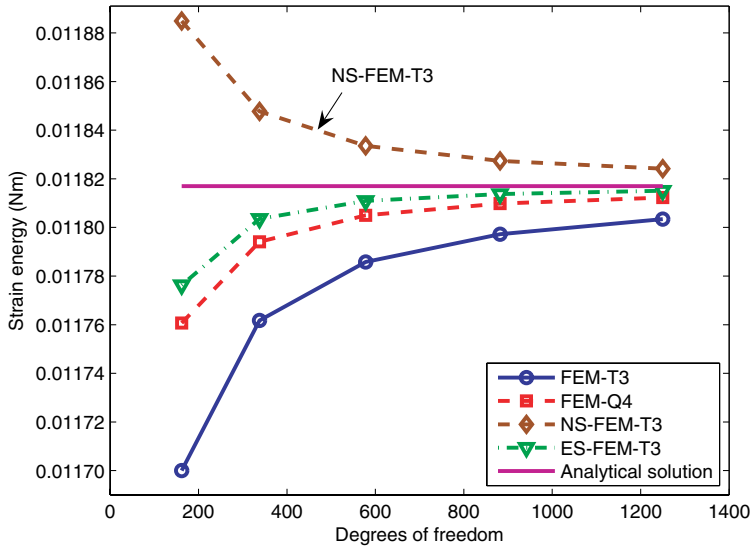

Fig. 13. Convergence of the strain energy solution of the NS-FEM-T3 in comparison with other methods for the infinite plate with a circular hole using the same distribution of nodes.

Table 5. Error in displacement norm obtained using different methods for the infinite plate with a circular hole using the same set of nodes.

	Mesh 1 8×8	Mesh 2 12×12	Mesh 3 16×16	Mesh 4 20×20	Mesh 5 24×24
h (m)	0.5468	0.3786	0.2895	0.2343	0.1969
FEM-T3	2.80 e-04	1.42 e-04	8.45 e-05	5.61 e-05	4.01 e-05
FEM-Q4	1.08 e-04	4.46 e-05	2.40 e-05	1.50 e-05	1.03 e-05
NS-FEM-T3	3.87 e-04	1.69 e-04	8.95 e-05	5.49 e-05	3.70 e-05
ES-FEM-T3	8.03 e-05	2.95 e-05	1.63 e-05	1.06 e-05	7.46 e-06

terms of convergence rate, except the FEM-T3, other models have a numerical rate slightly larger than the theoretical value of 2.0.

Table 6 and Fig. 15 compare the results of energy norm of the NS-FEM-T3 with those of the FEM and ES-FEM-T3. It is again seen that the NS-FEM-T3 stands out clearly. When the finest mesh ($h = 0.1969$ m) is used, the error of the NS-FEM-T3 is about 1/9 of the FEM-T3, 1/5 of the FEM-Q4, 1/3.5 of the FEM-T3-Re, and even 1/2 of the FEM-Q4-Re. In terms of convergence rate, all the S-FEM models performed much better than the FEM models, and all close to 2.0 and significantly above 1.0 that is the theoretical value of the weak formulation. This again shows that the S-FEM models are super-convergent. The NS-FEM-T3 stands out clearly with a rate of 1.97: a very strong super-convergence.

In overall, it is again seen that NS-FEM models possess four interesting properties of an equilibrium FEM model [Almeida Pereira (2008); Debongnie *et al.* (1995); Fraeijs De Veubeke (2001)]: (1) the strain energy is an upper bound of the

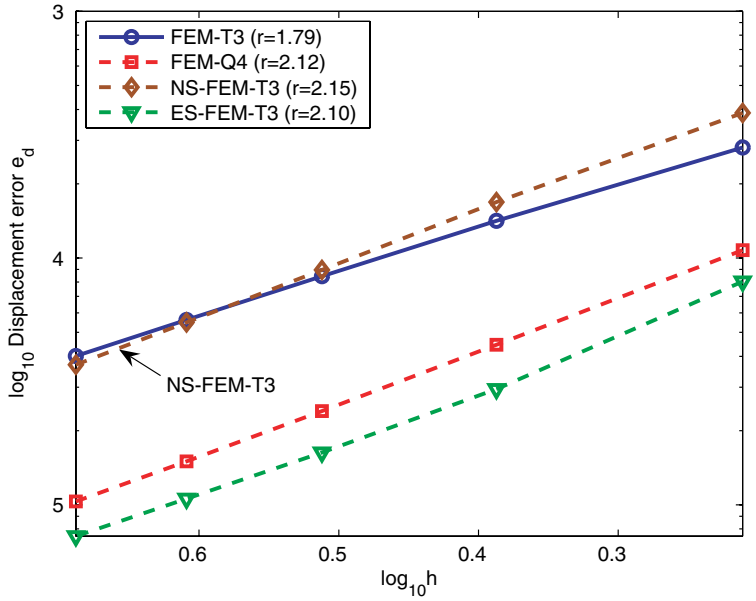

Fig. 14. Error in displacement norm for NS-FEM-T3 in comparison with those of other methods for the infinite plate with a circular hole using the same set of nodes.

Table 6. Error in energy norm obtained using different methods for the infinite plate with a circular hole using the same set of nodes.

	Mesh 1 8 × 8	Mesh 2 12 × 12	Mesh 3 16 × 16	Mesh 4 20 × 20	Mesh 5 24 × 24
h (m)	0.5468	0.3786	0.2895	0.2343	0.1969
FEM-T3	9.95 e-03	6.89 e-03	5.20 e-03	4.17 e-03	3.48 e-03
FEM-Q4	6.09 e-03	3.86 e-03	2.79 e-03	2.18 e-03	1.79 e-03
NS-FEM-T3	3.08 e-03	1.50 e-03	8.52 e-04	5.39 e-04	3.68 e-04
ES-FEM-T3	5.27 e-03	2.69 e-03	1.59 e-03	1.04 e-03	7.29 e-04
FEM-T3-Re	7.78 e-03	4.39 e-03	2.72 e-03	1.82 e-03	1.31 e-03
FEM-Q4-Re	5.22 e-03	2.72 e-03	1.61 e-03	1.05 e-03	7.41 e-04

exact solution; (2) it is immune naturally from the volumetric locking [Liu *et al.* (2009c)]; (3) the stress solutions are ultra-accurate and super-convergent; and (4) the displacement solutions are at the same level as those of FEM-T3 using the same distribution of nodes.

4.3. *3D Lame problem (hollow sphere problem)*

The 3D Lame problem consist of a hollow sphere with inner radius a =1 m, outer radius b = 2 m and subjected to internal pressure P = 100 N/m^2, as shown in Fig. 16. The analytical solution of the benchmark problem is available in polar

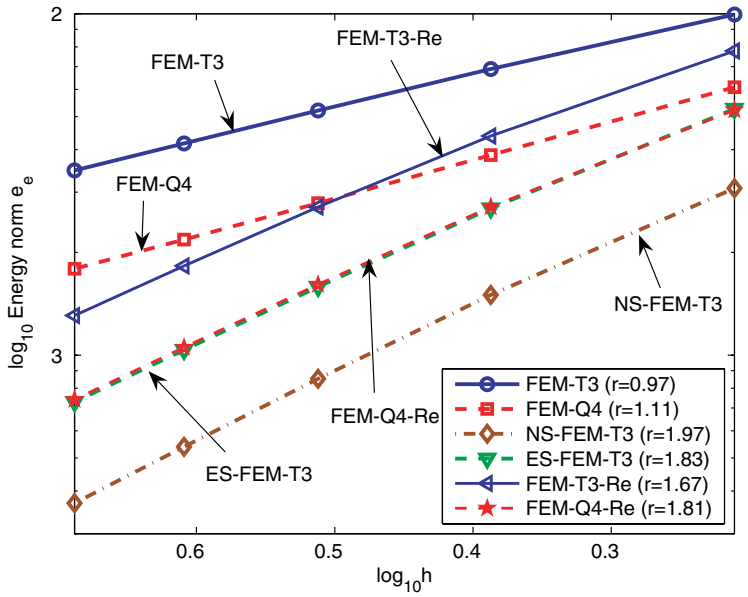

Fig. 15. Error in energy norm for NS-FEM-T3 in comparison with those of other methods for the infinite plate with a circular hole using the same set of nodes.

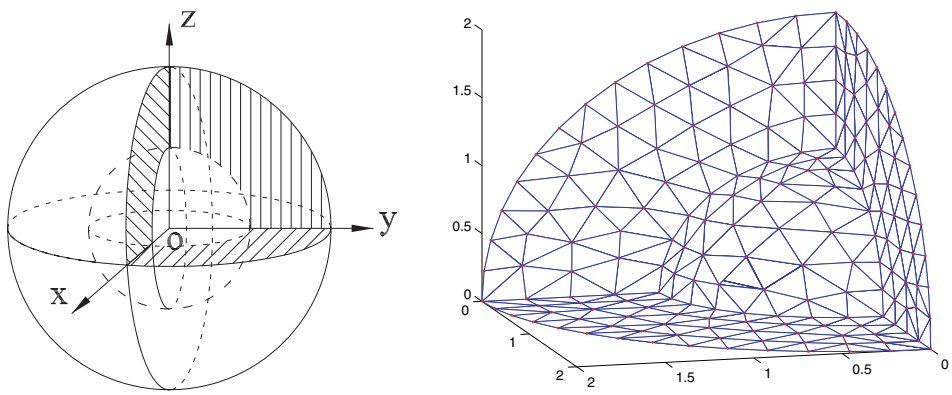

Fig. 16. Hollow sphere problem setting and its one-eighth model discretized using 4-node tetrahedral elements.

coordinate system [Timoshenko and Goodier (1970)]

$$u_r = \frac{Pa^3 r}{E(b^3 - a^3)}\left[(1-2\nu) + (1+\nu)\frac{b^3}{2r^3}\right],$$
$$\sigma_r = \frac{Pa^3(b^3 - r^3)}{r^3(a^3 - b^3)}; \quad \sigma_\theta = \frac{Pa^3(b^3 + 2r^3)}{2r^3(b^3 - a^3)}, \tag{32}$$

where r is the radial distance from the centroid to the point of interest of the sphere.

As the problem is spherically symmetrical, only one-eighth of the sphere shown in Fig. 16 is modeled, and the symmetry conditions are imposed on the three cutting symmetric planes. The material parameters of the problem are $E = 10^3\,\mathrm{N/m}^2$ and $v = 0.3$.

From Fig. 17, it is observed that all the computed displacements and stresses of the NS-FEM-T4 agree well with the analytical solutions. Table 7 and Fig. 18

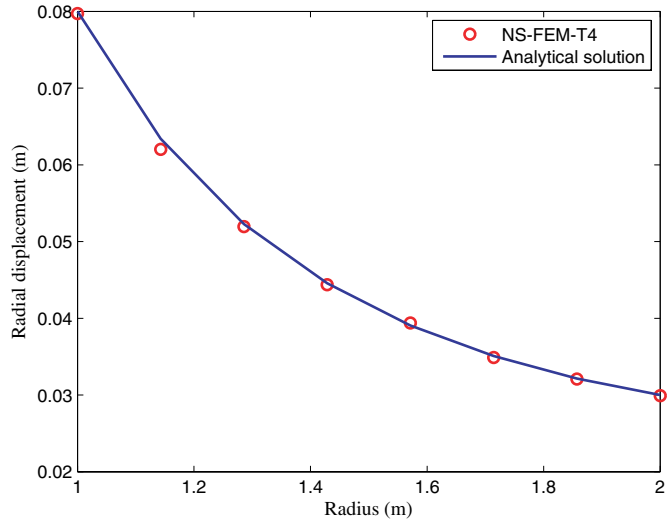

(a)

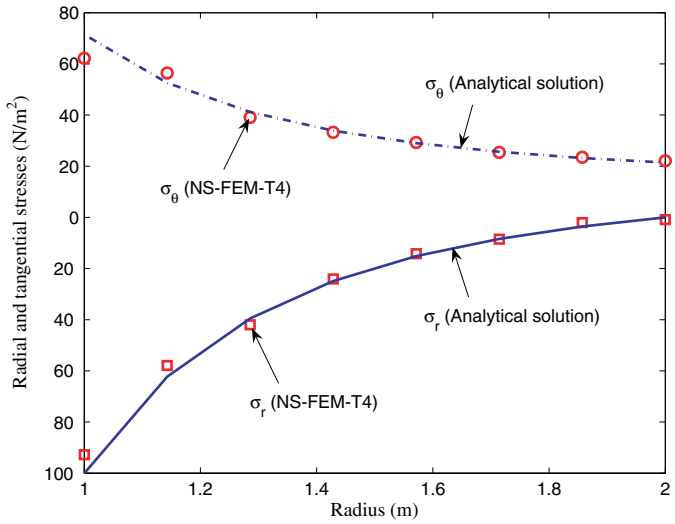

(b)

Fig. 17. (a) Radial displacement v (m); (b) Radial and tangential stresses ($\mathrm{N/m}^2$) for the hollow sphere subjected to inner pressure.

Table 7. Strain energy ($\times 10^{-2}$ Nm) obtained using different methods for the hollow sphere subjected to inner pressure.

	Mesh 1	Mesh 2	Mesh 3	Mesh 4	Analytical sol.
DOFs (T4)	1521	2337	3825	5814	
DOFs (H8)	1092	2535	3906	6951	
FEM-T4	5.9131	5.9986	6.0929	6.1387	6.3060
NS-FEM-T4	6.6227	5.5380	6.4580	6.4219	6.3060
FEM-H8	5.9827	6.1063	6.1668	6.2023	6.3060
FS-FEM-T4	6.0343	6.0955	6.1607	6.1906	6.3060

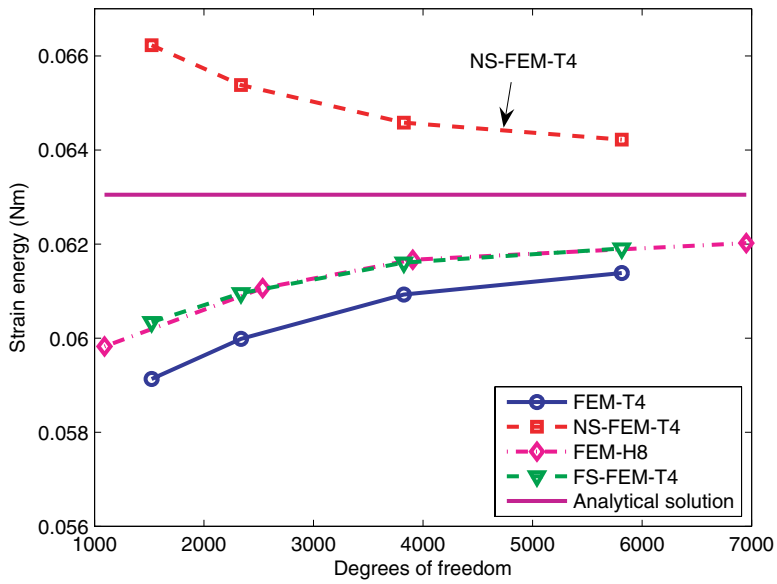

Fig. 18. Convergence of the strain energy solution of the NS-FEM-T4 in comparison with other methods for the hollow sphere subjected to inner pressure.

show the upper bound property in the strain energy of the NS-FEM-T4, while the FEM-T4 and FEM-H8 give the lower bounds.

Table 8 and Fig. 19 compare the solution error in displacement norm obtained using the NS-FEM-T4, together with those of the FEM-T4, FEM-H8 and FS-FEM-T4. It is seen that the FEM-H8, stands out clearly. When the third fine mesh for both T4 and H8 ($h \approx 0.156$) is used, the error of the FEM-H8 is about 1/3 of the NS-FEM-T4. The NS-FEM-T4 performed better than the FEM-T4, but only by a small margin. In terms of convergence rate, all the models have a numerical rate of around the theoretical value of 2.0.

Table 9 and Fig. 20 compare the results of energy norm of the NS-FEM-T4, together with those of the FEM-T4, FEM-H8, and FS-FEM-T4. It is again seen that the NS-FEM-T4 stand out clearly. When the third fine mesh for both T4 and

Table 8. Error in displacement norm obtained using different methods for the hollow sphere subjected to inner pressure.

	Mesh 1	Mesh 2	Mesh 3	Mesh 4
h (T4)	0.2193	0.1878	0.1565	0.1342
h (H8)	0.2535	0.1840	0.1563	0.1267
FEM-T4	4.06 e-03	3.12 e-03	2.07 e-03	1.58 e-03
NS-FEM-T4	3.68 e-03	2.76 e-03	1.88 e-03	1.48 e-03
FEM-H8	2.26 e-03	1.35 e-03	7.92 e-04	5.44 e-04
FS-FEM-T4	3.03 e-03	2.30 e-03	1.50 e-03	1.14 e-03

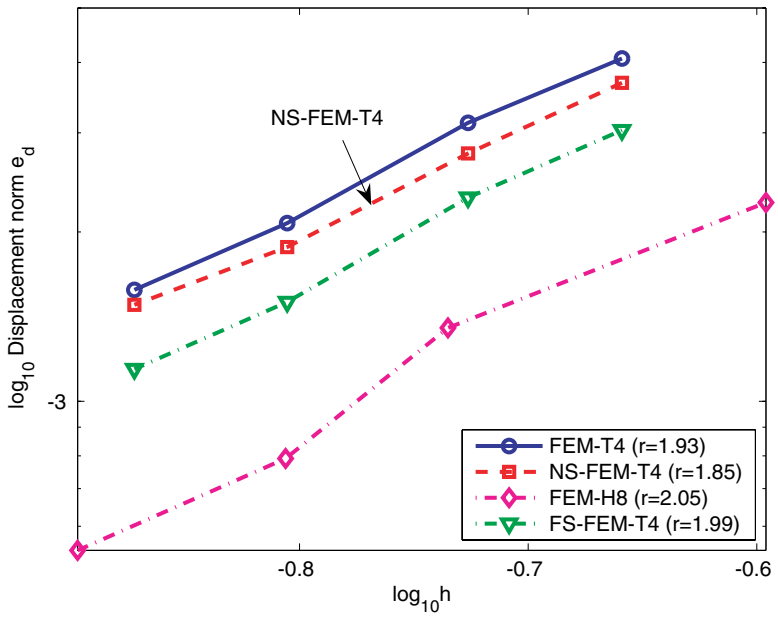

Fig. 19. Error in displacement norm for the NS-FEM-T4 solution in comparison with those of other methods for the hollow sphere subjected to inner pressure.

Table 9. Error in energy norm obtained using different methods for the hollow sphere subjected to inner pressure.

	Mesh 1	Mesh 2	Mesh 3	Mesh 4
h (T4)	0.2193	0.1878	0.1565	0.1342
h (H8)	0.2535	0.1840	0.1563	0.1267
FEM-T4	5.89 e-01	5.13 e-01	4.19 e-01	3.63 e-01
NSFEM-T4	2.09 e-01	1.73 e-01	1.26 e-01	1.08 e-01
FEM-H8	5.51 e-01	4.22 e-01	3.42 e-01	2.85 e-01
FS-FEM-T4	3.75 e-01	3.03 e-01	2.24 e-01	1.86 e-01
FEM-T4-Re	4.20 e-01	3.39 e-01	2.51 e-01	2.08 e-01
FEM-H8-Re	4.90 e-01	3.31 e-01	2.56 e-01	1.98 e-01

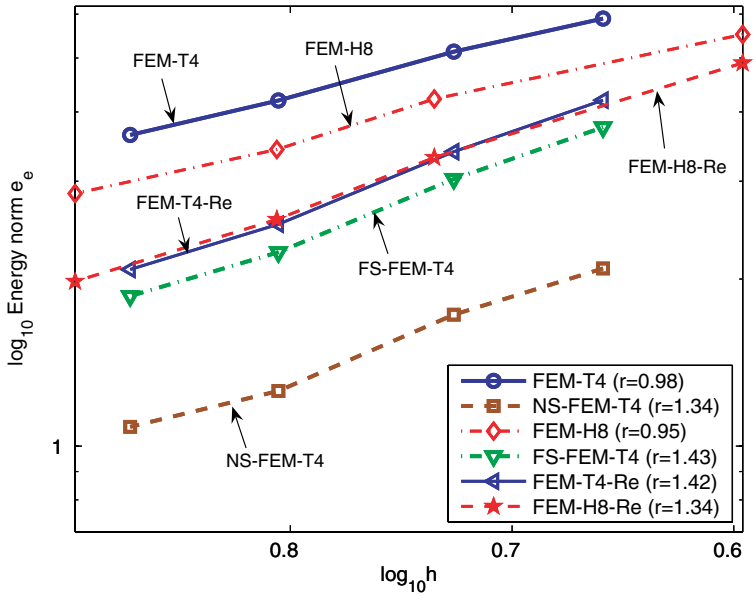

Fig. 20. Error in energy norm for the NS-FEM-T4 solution in comparison with those of other methods for the hollow sphere subjected to inner pressure.

H8 ($h \approx 0.156$) is used, the error of the NS-FEM-T4 is about 2/7 of the FEM-T4, 2/5 of the FEM-H8, 1/2 of the FEM-T4-Re, 1/2 of the FEM-H8-Re, and 3/5 of the FS-FEM-T4. In terms of convergence rate, the NS-FEM-T4 stands out clearly with a rate of 1.34, while the rates of both FEM-T4 and FEM-H8 are slightly below the theoretical value of 1.0.

Figure 21 plots the error in displacement norm against Poisson's ratio changing from 0.4 to 0.4999999 by using tetrahedral elements (507 nodes). The results show that the NS-FEM-T4 is naturally immune from the volumetric locking, while the FEM-T4 is subjected to the volumetric locking resulting in a drastic accuracy lose in the numerical solutions.

In overall, it is again seen that the NS-FEM-T4 model also possesses four interesting properties that are similar to an equilibrium FEM model: (1) the strain energy is an upper bound of the exact solution; (2) it is immune naturally from the volumetric locking; (3) the stress solutions are ultra-accurate and super-convergent; and (4) the displacement solutions are at the same level as that of FEM-T4 using the same mesh.

4.4. *3D cubic cantilever: An analysis about the upper bound property*

Consider a 3D cantilever of cubic shape, subjected to a uniform pressure on its upper face as shown in Fig. 22. The exact solution of the problem is unknown. By

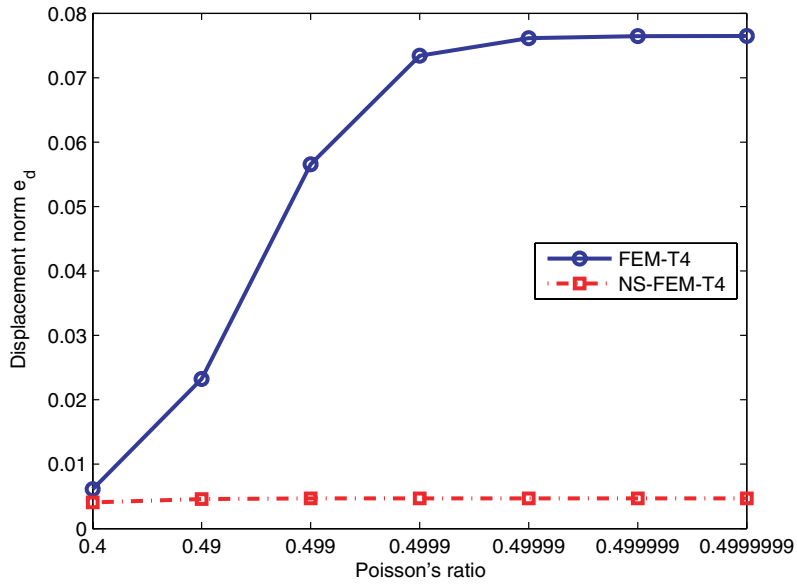

Fig. 21. Displacement norm vs. different Poisson's ratios for the hollow sphere subjected to inner pressure (507 nodes).

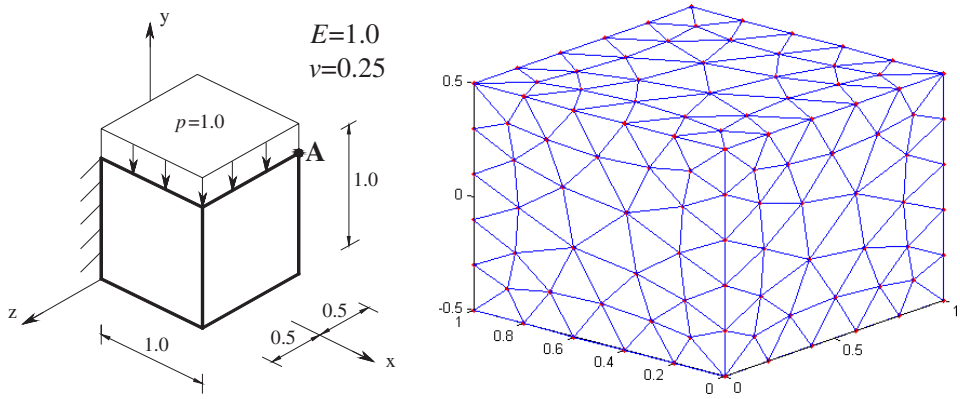

Fig. 22. A 3D cubic cantilever subjected to a uniform pressure on the top surface, and a mesh with four-node tetrahedral elements.

incorporating the solutions of hexahedral super-element elements and the procedure of Richardson's extrapolation, Almeida Pereira [2008] gave an approximation of the exact strain energy to be 0.950930. In addition, using standard FEM and a very fine mesh with 30,204 nodes and 20,675 ten-node tetrahedron elements, another reference solution of the strain energy is 0.9486. From this reference, the deflection at point A $(1.0, 1.0, -0.5)$ is 3.3912.

Table 10. Strain energy obtained using different methods for the 3D cubic cantilever problem subjected to a uniform pressure.

	Mesh 1	Mesh 2	Mesh 3	Mesh 4	Mesh 5	Reference sol.
DOFs (T4)	714	1221	2073	2856	4782	
DOFs (H8)	648	1029	1536	2187	3993	
FEM-T4	0.8572	0.8818	0.8978	0.9088	0.9190	0.9509
NS-FEM-T4	1.0059	0.9882	0.9808	0.9791	0.9704	0.9509
FEM-H8	0.8999	0.9116	0.9195	0.9251	0.9323	0.9509
FS-FEM-T4	0.8801	0.8989	0.9111	0.9206	0.9274	0.9509

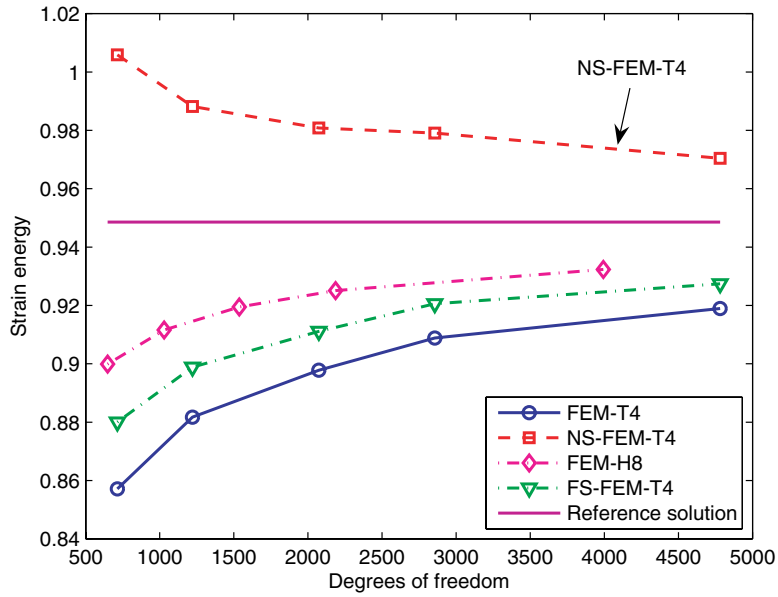

Fig. 23. Convergence of the strain energy solution of the NS-FEM-T4 in comparison with other methods of the 3D cubic cantilever problem subjected to a uniform pressure.

Table 10 and Fig. 23 confirm the upper bound property on the strain energy of the NS-FEM-T4 and the lower bound property of the FEM-T4 and FEM-H8 for this 3D problem. Table 11 and Fig. 24 show the convergence of deflection at point A $(1.0, 1.0, -0.5)$. The results also show the upper bound property for the displacement solution of the NS-FEM-T4 and the lower bound property of the FEM-T4 and FEM-H8.

4.5. *A 3D automotive part (rim): An analysis about the upper bound property*

Consider a typical 3D rim used in automotive industry as shown in Fig. 25. The rim is of inner radius 2 m, outer radius 19 m and a thickness of 3 m. It is constrained

Table 11. Deflection at point A $(1.0, 1.0, -0.5)$ obtained using different methods for the 3D cubic cantilever problem subjected to a uniform pressure.

	Mesh 1	Mesh 2	Mesh 3	Mesh 4	Mesh 5	Reference sol.
DOFs (T4)	714	1221	2073	2856	4782	
DOFs (H8)	648	1029	1536	2187	3993	
FEM-T4	3.0780	3.1752	3.2341	3.2732	3.3050	3.3912
NS-FEM-T4	3.5912	3.5418	3.4943	3.4818	3.4577	3.3912
FEM-H8	3.2523	3.2875	3.3107	3.3269	3.3474	3.3912
FS-FEM-T4	3.1669	3.2390	3.2800	3.3128	3.3324	3.3912

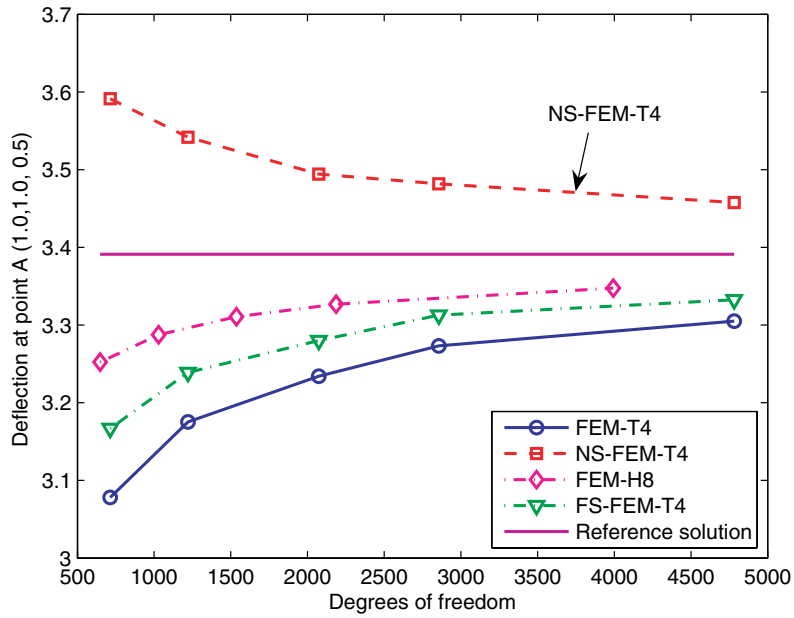

Fig. 24. Convergence of the deflection solution at point $A(1.0, 1.0, -0.5)$ of the NS-FEM-T4 in comparison with other methods of the cubic cantilever subjected to a uniform pressure.

in three dimensions along the inner annulus and a uniform pressure of $40\,\mathrm{KN/m^2}$ is applied on the outer annulus of 60°. The material parameters of the problem are $E = 3 \times 10^7\,\mathrm{N/m^2}$ and $v = 0.3$.

Note that for this problem, a discretization using eight-node hexahedral elements (H8) is impossible due to the complicated geometry of the problem. Therefore, we just use NS-FEM-T4, FEM-T4, and FS-FEM-T4 using four-node tetrahedral elements (T4) to compute this problem.

As no analytical solution is available for this problem, a reference solution is obtained using the FEM-T4 with a very fine mesh including 17,761 nodes (53,283 DOFs) and 82,991 elements.

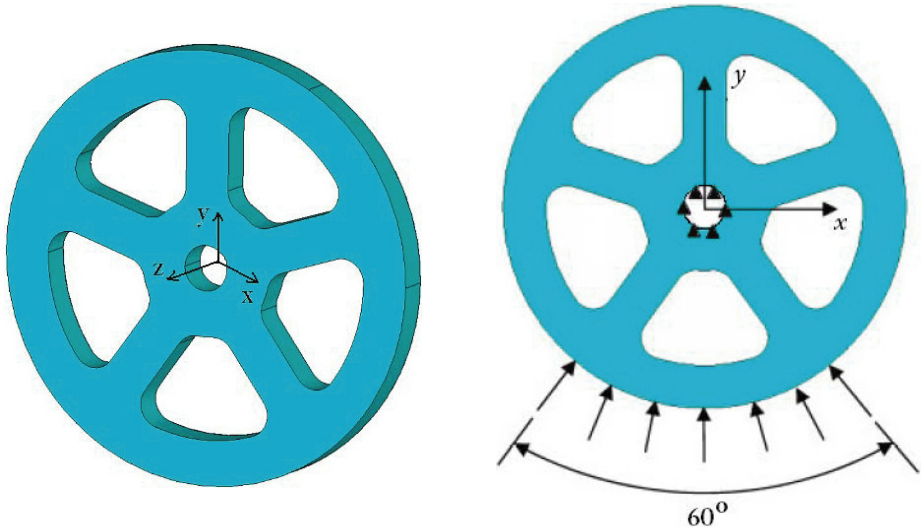

Fig. 25. Simplified model of an 3D automotive rim.

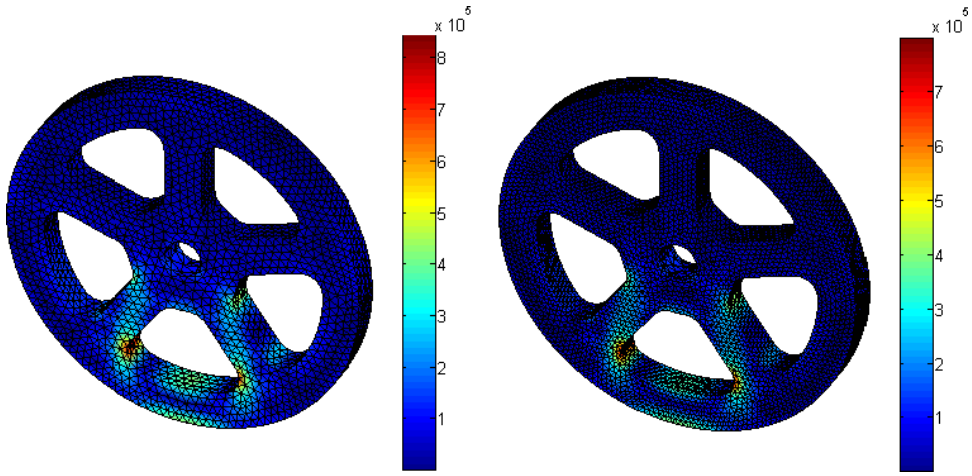

Fig. 26. Distribution of von-Mises stress of the 3D automotive rim; (a) NS-FEM-T4 using 18,504 DOFs; (b) FEM-T4 using 53,283 DOFs.

Figure 26 shows the distribution of von-Mises stress using NS-FEM-T4 with 18,504 DOFs compared with that using FEM-T4 with 53,283 DOFs. Although DOFs of NS-FEM-T4 are much smaller than that of FEM-T4, the color-bar of NS-FEM-T4 has higher max level than that of FEM-T4. This implied that the stress distribution of NS-FEM-T4 is sharper and concentrated than that of FEM-T4. This result again confirms the super accuracy of stress solution of NS-FEM.

Table 12. Strain energy obtained using different methods for the 3D automotive part problem ($\times 10^5$ Nm).

	Mesh 1	Mesh 2	Mesh 3	Mesh 4	Mesh 5	Reference solution using FEM-T4
DOFs (T4)	3777	5412	8607	12,189	18,504	53,283
FEM-T4	1.1654	1.1911	1.2595	1.3076	1.3439	1.4062
NSFEM-T4	1.7316	1.6784	1.6307	1.5873	1.5590	1.4062
FS-FEM-T4	1.2439	1.2647	1.3219	1.3583	1.3855	1.4062

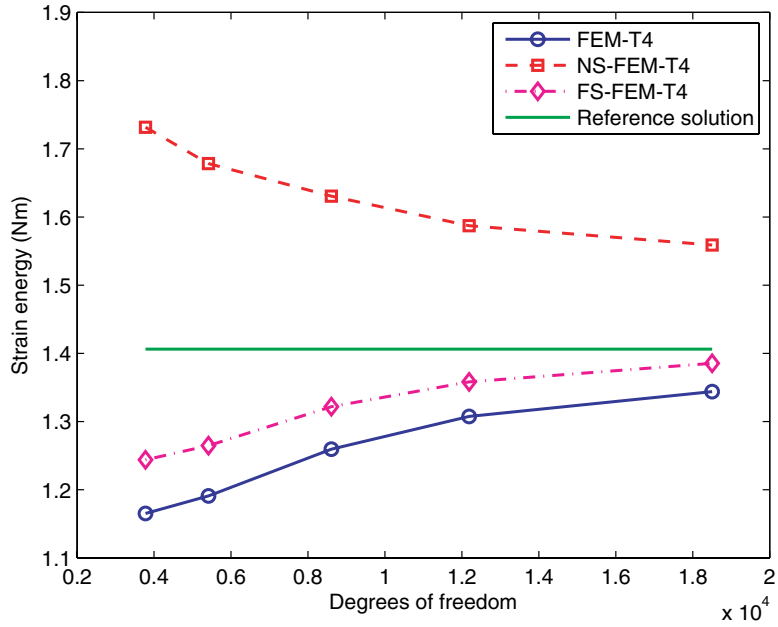

Fig. 27. Convergence of the strain energy solution of the NS-FEM-T4 in comparison with other methods of the 3D automotive rim.

Table 12 and Fig. 27 again confirm the upper bound property on the strain energy of the NS-FEM-T4 and the lower bound property of the FEM-T4 for this 3D problem.

5. Conclusion

Apart from the upper bound property in the strain energy and natural immunization from the volumetric locking presented in the original paper of NS-FEM [Liu *et al.* (2009c)], in this paper, we (1) extend the NS-FEM to 3D problems using tetrahedral elements (NS-FEM-T4), (2) reconfirm the upper bound and free from the volumetric locking properties for 3D problems, and (3) explore further other properties of

NS-FEM for both 2D and 3D problems by considering fully the error norms in both energy and displacement. The results in the paper show that NS-FEM possesses two other interesting properties of an equilibrium FEM model such as: (1) ultra-accuracy and super-convergence of stress solutions; (2) the same accuracy of displacement solutions as that of the standard FEM using the same mesh.

With first additional property: ultra-accuracy and super-convergence of stress solutions studied in this paper, NS-FEM now has very promising abilities to further apply effectively in many applications: (1) NS-FEM can immune naturally from volumetric locking for nearly incompressible materials and can be applied effectively to solve the nonlinear problems which require the high accuracy of stress solutions at nodes; (2) Together with the standard FEM, NS-FEM now can bound the numerical solutions from both upper and lower bounds; (3) The recovery stress (or strain) field used in NS-FEM can be used as a representation of exact stress (or strain) field in the adaptive analysis or error estimations [Nguyen-Thoi *et al.* (2009c)]; (4) In particular, NS-FEM can use the three-node linear triangular element for 2D problems and four-node linear tetrahedral element for 3D problems which can be generated automatically for 2D and 3D complicated geometries and (5) The numerical implementation of NS-FEM is straightforward and much simpler than that of equilibrium FEM models.

References

Almeida Pereira, O. J. B. [2008] Hybrid equilibrium hexahedral elements and super-elements, *Commun. Numer. Methods Eng.* **24**(2), 157–165.

Bathe, K. J. [1996] *Finite Element Procedures* (MIT Press/Prentice Hall, Cambridge, MA: Englewood Cliffs, NJ).

Bordas, S., Rabczuk, T., Nguyen-Xuan, H., Nguyen Vinh, P., Natarajan, S., Bog, T., Do Minh, Q. and Nguyen Vinh, H. [2009] Strain smoothing in FEM and XFEM, *Comput. Struct.*, doi:10.1016/j.compstruc.2008.07.006.

Chen, J. S., Wu, C. T., Yoon, S. and You, Y. [2001] A stabilized conforming nodal integration for Galerkin meshfree method, *Int. J. Numeri. Methods Eng.* **50**, 435–466.

Cui, X. Y., Liu, G. R., Li, G. Y., Zhao, X., Nguyen-Thoi, T. and Sun, G. Y. [2008] A smoothed finite element method (SFEM) for linear and geometrically nonlinear analysis of plates and shells, *Comput. Model. Eng. Sci.* **28**(2) 109–125.

Dai, K. Y. and Liu, G. R. [2007] Free and forced analysis using the smoothed finite element method (SFEM), *J. Sound Vib.* **301**, 803–820.

Dai, K. Y., Liu, G. R. and Nguyen-Thoi, T. [2007] An n-sided polygonal smoothed finite element method (nSFEM) for solid mechanics, *Finite Elem. Anal. Des.* **43**, 847-860.

Debongnie, J. F., Zhong, H. G. and Beckers, P. [1995] Dual analysis with general boundary conditions, *Comput. Methods Appl. Mech. Eng.* **122**, 183–192.

Dohrmann, C. R., Heinstein, M. W., Jung, J., Key, S. W. and Witkowski, W. R. [2000] Node-based uniform strain elements for three-node triangular and four-node tetrahedral meshes, *Int. J. Numer. Methods Eng.* **47**, 1549–1568.

Felippa, C. [2009] *Introductions to Finite Element Methods* (ASEN 5007), Chapter 28: Stress Recovery, http://www.colorado.edu/engineering/CAS/courses.d/IFEM.d/

Fraeijs De Veubeke, B. [2001] Displacement and equilibrium models in the finite element Method, in Stress Analysis, eds. Zienkiewicz, O. C. and Holister, G. (John Wiley and

Sons, 1965) Chap. 9, pp. 145–197. Reprinted in *Int. J. Numer. Methods Eng.* **52**, 287–342.

Johnson, C. and Mercier, B. [1978] Some equilibrium finite element methods for two-dimensional elasticity problems, *Numerische Mathematik* **30**(1), 103–116.

Liu, G. R., Dai, K. Y. and Nguyen-Thoi, T. [2007] A smoothed finite element method for mechanics problems, *Comput. Mech.* **39**, 859–877.

Liu, G. R., Li, Y., Dai, K. Y., Luan, M. T. and Xue, W. [2006] A Linearly conforming radial point interpolation method for solid mechanics problems, *Int. J. Comput. Methods* **3**(4), 401–428.

Liu, G. R., Nguyen-Thoi, T., Dai, K. Y. and Lam, K. Y. [2007] Theoretical aspects of the smoothed finite element method (SFEM), *Int. J. Numer. Methods Eng.* **71**, 902–930.

Liu, G. R., Nguyen-Thoi, T. and Lam, K. Y. [2008] A novel alpha finite element method (αFEM) for exact solution to mechanics problems using triangular and tetrahedral elements, *Comput. Methods Appl. Mech. Eng.* **197**, 3883–3897.

Liu, G. R., Nguyen-Thoi, T. and Lam, K. Y. [2009a] An edge-based smoothed finite element method (ES-FEM) for static, free and forced vibration analyses of solids, *J. Sound Vib.* **320**, 1100–1130.

Liu, G. R., Nguyen-Thoi, T., Nguyen-Xuan, H., Dai, K. Y. and Lam, K. Y. [2009b] On the essence and the evaluation of the shape functions for the smoothed finite element method (SFEM) (Letter to Editor), *Int. J. Numer. Methods Eng.* **77**, 1863–1869.

Liu, G. R., Nguyen-Thoi, T., Nguyen-Xuan, H. and Lam, K. Y. [2009c] A node-based smoothed finite element method for upper bound solution to solid problems (NS-FEM), *Comput. Struct.* **87**, 14–26.

Liu, G. R. and Quek, S. S. [2003] *The Finite Element Method: A Practical Course* (Butterworth Heinemann, Oxford).

Liu, G. R. and Zhang, G. Y. [2008] Upper bound solution to elasticity problems: A unique property of the linearly conforming point interpolation method (LC-PIM), *Int. J. Numer. Methods Eng.* **74**, 1128–1161.

Liu, G. R., Zhang, G. Y., Dai, K. Y., Wang, Y. Y., Zhong, Z. H., Li, G. Y. and Han, X. [2005] A linearly conforming point interpolation method (LC-PIM) for 2D solid mechanics problems, *Int. J. Comput. Methods* **2**(4), 645–665.

Nguyen-Thanh, N., Rabczuk, T., Nguyen-Xuan, H. and Bordas, S. [2008] A smoothed finite element method for shell analysis, *Comput. Methods Appl. Mech. Eng.* **198**, 165–177.

Nguyen-Thoi, T., Liu, G. R., Dai, K. Y. and Lam, K. Y. [2007] Selective smoothed finite element method, *Tsinghua Sci. Technol.* **12**(5), 497–508.

Nguyen-Thoi, T, Liu, G. R., Lam, K. Y. and Zhang, G. Y. [2009a] A face-based smoothed finite element method (FS-FEM) for 3D linear and nonlinear solid mechanics problems using 4-node tetrahedral elements, *Int. J. Numer. Methods Eng.* **78**, 324–353.

Nguyen-Thoi, T., Liu, G. R. and Nguyen-Xuan, H. [2009b] An n-sided polygonal edge-based smoothed finite element method (nES-FEM) for solid mechanics, *Commun. Numer. Methods Eng.*, accepted.

Nguyen-Thoi, T., Liu, G. R., Nguyen-Xuan, H. and Nguyen-Tran, C. [2009c] Adaptive analysis using the node-based smoothed finite element method (NS-FEM), *Communi. Numer. Meth. Eng*, doi: 10.1002/cnm.1291.

Nguyen-Thoi, T., Liu, G. R., Vu-Do, H. C. and Nguyen-Xuan, H. [2009d] An edge-based smoothed finite element method (ES-FEM) for visco-elastoplastic analyses in 2D solids using triangular mesh, *Comp. Mech.* **45**, 23–44.

Nguyen-Thoi, T., Liu, G. R., Vu-Do, H. C. and Nguyen-Xuan, H. [2009e] A face-based smoothed finite element method (FS-FEM) for visco-elastoplastic analyses of 3D solids using tetrahedral mesh, *Comput. Methods Appl. Mech. Eng.* **198**, 3479–3498.

Nguyen-Van, H., Mai-Duy, N. and Tran-Cong, T. [2008] A smoothed four-node piezoelectric element for analysis of two-dimensional smart structures, *Comput. Model. Eng. Sci.* **23**(3) 209–222.

Nguyen-Xuan, H., Bordas, S. and Nguyen-Dang, H. [2008a] Smooth finite element methods: Convergence, accuracy and properties, *Int. J. Numer. Methods Eng.* **74**, 175–208.

Nguyen-Xuan, H., Bordas, S. and Nguyen-Dang, H. [2008b] Addressing volumetric locking and instabilities by selective integration in smoothed finite elements, *Commun. Numer. Methods Eng.* **25**, 19–34.

Nguyen-Xuan, H., Liu, G. R., Nguyen-Thoi, T. and Nguyen-Tran, C. [2009a] An edge-based smoothed finite element method (ES-FEM) for analysis of two-dimensional piezoelectric structures, *Smart Mater. and Struct.* **18**, 065015 (12pp).

Nguyen-Xuan, H., Liu, G. R., Thai-Hoang, C. and Nguyen-Thoi, T. [2009b] An edge-based smoothed finite element method with stabilized discrete shear gap technique for analysis of Reissner-Mindlin plates, *Comput. Methods Appl. Mech. Eng.*, document doi:10.1016/j.cma.2009.09.001.

Nguyen-Xuan, H. and Nguyen-Thoi, T. [2009] A stabilized smoothed finite element method for free vibration analysis of Mindlin-Reissner plates, *Commun. Numer. Methods Eng.* **25**, 882–906.

Nguyen-Xuan, H., Rabczuk, T., Bordas, S. and Debongnie, J. F. [2008] A smoothed finite element method for plate analysis, *Comput. Methods Appl. Mech. Eng.* **197**, 1184–1203.

Timoshenko, S. P. and Goodier, J. N. [1970] *Theory of Elasticity*, 3rd edition (McGraw-Hill, New York).

Tran, Thanh. Ngoc., Liu, G. R., Nguyen-Xuan, H. and Nguyen-Thoi, T. [2009] An edge-based smoothed finite element method for primal-dual shakedown analysis of structures, *Int. J. Numeri. Methods Eng.*, doi:10.1002/nme.2804.

Yoo, J. W., Moran, B. and Chen, J. S. [2004] Stabilized conforming nodal integration in the natural-element method, *Int. J. Numer. Methods Eng.* **60**, 861–890.

Zienkiewicz, O. C. and Taylor, R. L. [2000] *The Finite Element Method*, 5th edition (Butterworth Heinemann, Oxford).

Zienkiewicz, O. C. and Zhu, J. Z. [1992a] The superconvergence patch recovery and a posteriori error estimates. Part 1: The recovery techniques, *Int. J. Numeri. Methods Eng.* **33**, 1331–1364.

Zienkiewicz, O. C. and Zhu, J. Z. [1992b] The superconvergence patch recovery and a posteriori error estimates. Part 2: Error estimates and adaptivity, *Int. J. Numer. Methods Eng.* **33**, 1365–1382.